Emerging anticancer therapeutic modalities brought by gold complexes: overview and perspectives

Michèle Salmain, Benoit Bertrand

Emerging anticancer therapeutic modalities brought by gold complexes: overview and perspectives

Michèle Salmain[a] and Benoît Bertrand[a]*

[a] Sorbonne Université, CNRS, Institut Parisien de Chimie Moléculaire (IPCM UMR 8232), F-75005 Paris, France

Email corresponding author: benoit.bertrand@sorbonne-universite.fr

Abstract

The medicinal chemistry of gold has experienced an exponential development since the 2000s. For long, the mechanisms of action of gold complexes have been limited to direct coordination of the gold ion or supramolecular interactions of the whole gold complex with biomolecules. In the recent years, other modes of action of gold-based drug candidates have emerged. Herein, we review these new modalities, including photo-induced cytotoxicity, selective protein modification and *in cellulo* catalysis.

Keywords

Gold, cancer, phototherapy, protein labeling, intracellular catalysis

1. Introduction

At the end of the XIXth century, the German physician Robert Koch reported the use of $K[Au(CN)_2]$ for the treatment of tuberculosis. Although its efficacy was heavily debated and further replaced by streptomycin, it represented the starting point of the modern use of gold-based compounds in medicine.[1] During the XXth century, gold-based polymeric compounds such as sodium aurothiomalate and aurothioglucose and orally available drug auranofin (Figure 1) were clinically used for the treatment of rheumatoid arthritis.[2] As such, when it became necessary to circumvent problems of resistance and heavy side effects, isoelectronic Au(III) complexes appeared as promising alternatives to platinum-based anticancer chemotherapeutic agents[3]. Moreover, auranofin is currently in repurposing investigations by undergoing clinical trials for various types of cancer, including ovarian cancer and leukemia.[4–6] In this context, both Au(I) and Au(III) complexes have attracted an exponentially growing interest in the last decades regarding the development of new anticancer drug candidates and the field has been abundantly reviewed during the last 5 years.[7–13] It is worth noting that beyond their anticancer properties, gold complexes have also demonstrated promising antibacterial,[14] antiparasitic,[15] antifungal[16] and antiviral[17] properties which topics are beyond the scope of the present review.

Interestingly, while the well-recognized target of cisplatin and its derivatives is DNA *via* the direct bonding of the Pt(II) center to puric bases such as guanines,[18] the mechanism of gold-based complexes appears to be very different since it mostly involves interactions with proteins and enzymes.[19] The vast majority of the gold complexes can be divided into two categories according to their reactivity. On one side, Au complexes presenting hydrolysable (exchangeable) ligands such as halogenides, carboxylates, thiolates (as for auranofin) will react by direct coordination of the gold atom to the target. Due to the soft nature of gold cations, which is even more pronounced for Au(I), gold complexes have been reported to interact with their targets by direct coordination of the Au center to sulfur- and selenium-containing residues, i.e. cysteines, methionines and

selenocysteines.[19] In this category, are found Au(I)-PR_3/NHC (Figure 1),[20,21] Au(III)-dithiocarbamates,[22] (N^N)[23] and cyclometalated complexes[24–27] (Figure 1). Different potential targets for reactive gold complexes have been identified, among which thioredoxin reductase (TrxR), which is involved in the cellular redox balance,[28] glutathione-S-transferase (GST), involved in cisplatin resistance,[29] the 20S subunit of proteasome[30], zinc-finger enzymes such as poly-ADP-ribose polymerase 1 (PARP-1), involved in DNA repair mechanisms,[31,32] or aqua(glycero)porins, some trans-membrane channels for water and glycerol.[33] The second main category comprises structural cationic complexes including stable ligands that prevent the possibility of direct coordination of the gold atom. These complexes interact with their targets *via* weak interactions such as π-stacking or electrostatic interactions as was demonstrated in the cases of the non-canonical G-quadruplex DNA structures,[34,35] and topoisomerase I, an enzyme involved in DNA cleavage and reannealing.[36] In this category one can find $[Au(I)\text{-}(NHC)_2]^+$,[37–39] $[(C^N^C)Au\text{-}(NHC)]^+$,[36,40,41] $[(C^N^N^C)Au]^+$[42] and $[Au(porphyrin)]^+$[43] (Figure 1).

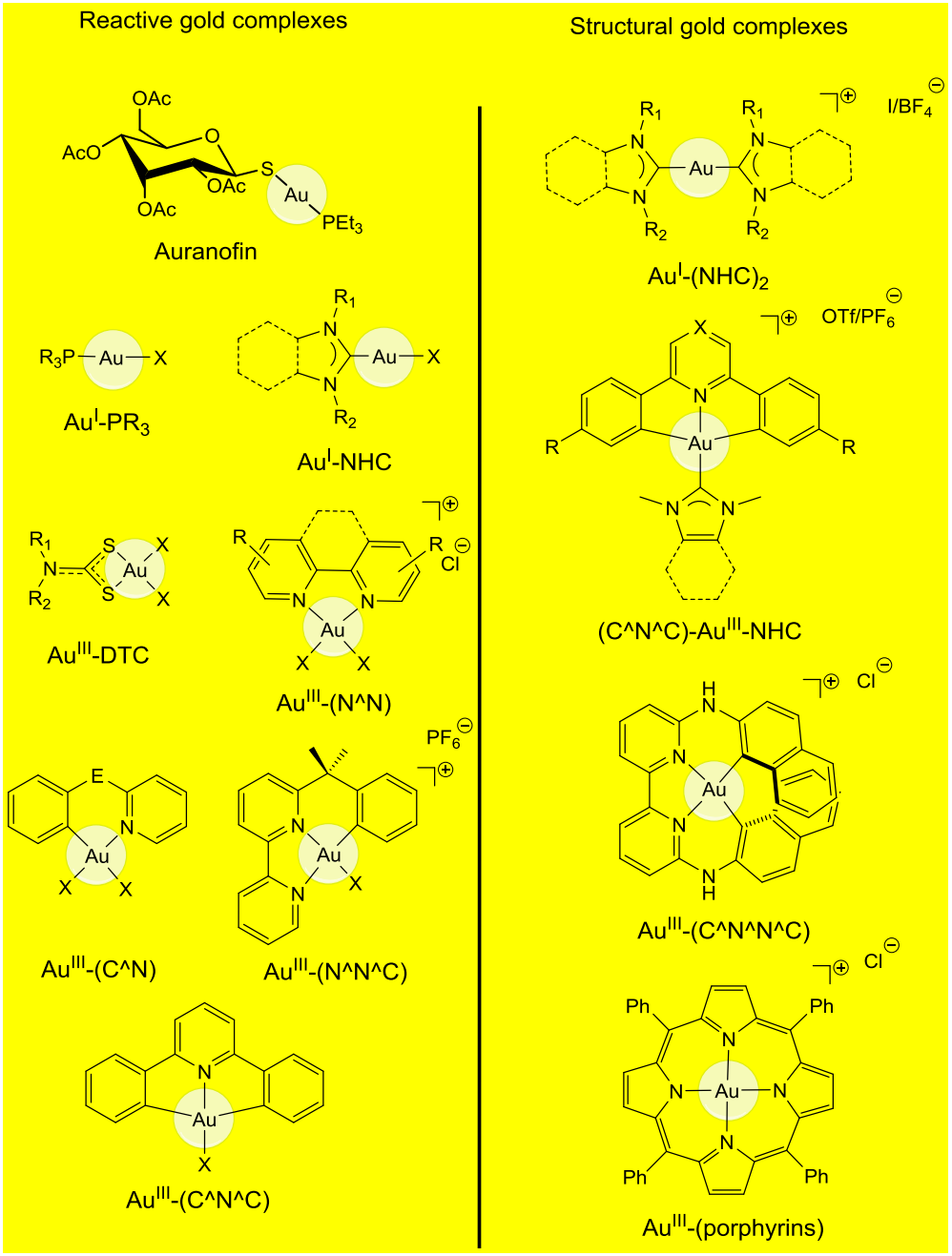

Figure 1. Examples of the main families of reactive and structural gold-based anticancer drug candidates

One of the main limitations of most gold-based anticancer drug candidates, common to the platinum-based drugs, is the generally low selectivity of the gold complexes for cancer cells. To bypass this shortcoming, different strategies have been explored such as vectorizing the gold complexes toward the desired cancer cells by conjugation of peptides,[44] aptamers,[45] vitamins,[46,47] or antibodies,[48] or to incorporate the gold complexes into nanocarriers.[13] In the recent years, beyond the classical mode of action of gold-based complexes, new therapeutic modalities have emerged to improve the selectivity and the efficacy of gold-based therapies. The present review will discuss the latest developments in the emerging gold-based therapeutic modalities which include gold-based photoactive therapies, selective protein modification and gold-based *in cellulo / in vivo* catalysis (Figure 2).

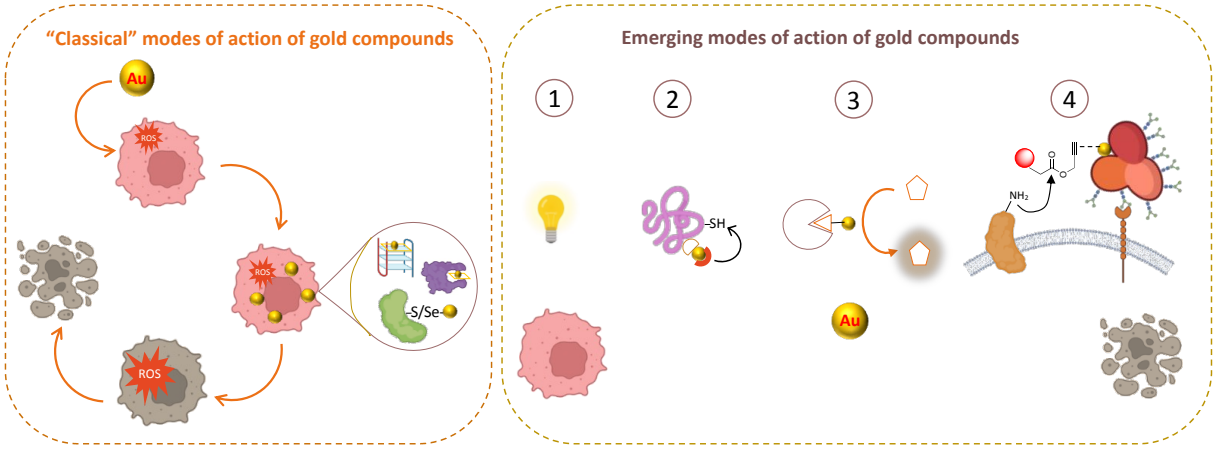

Figure 2. Schematic representation of traditional and emerging modes of action of gold compounds in cancer therapy. 1) Phototherapy; 2) gold-based protein chemistry; 3) gold-based artificial metalloenzymes; 4) SeCT

2. Gold-based complexes for photo-induced anticancer therapy

Light-induced therapies can be divided into two families, namely photodynamic therapy (PDT) and photoactivated chemotherapy (PACT). PDT relies on the formation of reactive oxygen species (ROS) upon irradiation by energy transfer from a photosensitizer to molecular oxygen. The most common ROS produced in PDT is singlet oxygen ($^1O_2$) generated by energy transfer from a triplet excited state of the photosensitizer induced by an intersystem crossing (ISC) mechanism from an excited singlet state (Figure 3A). Highly reactive $^1O_2$ will trigger oxidative damages to DNA, unsaturated lipids and proteins leading to cell death.[49] On the other hand, PACT pharmacophores rely on the photoactivation of a prodrug generating a reactive metabolite able to directly interact with biomolecules to trigger cell death (Figure 3B).

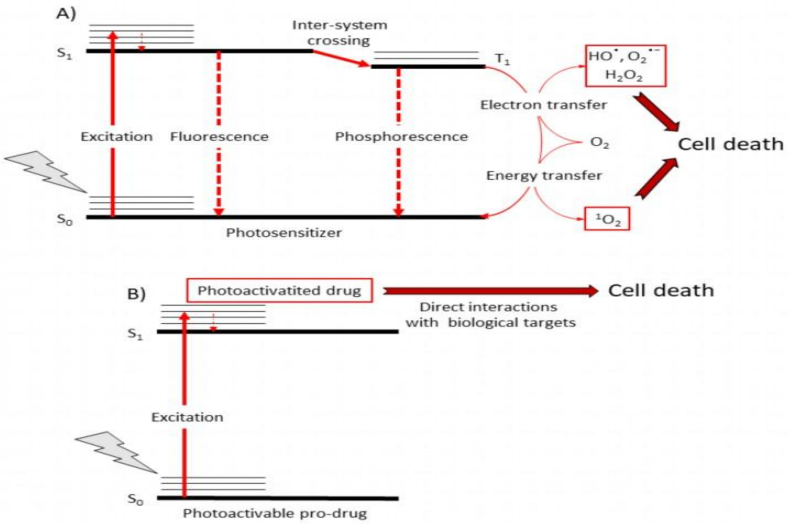

Figure 3. Mechanisms of A) Photodynamic therapy and B) Photoactivated chemotherapy

PDT is an FDA-approved therapeutic modality since the 90's for the treatment of various types of cancer including non-small lung cancer, head and neck cancer or bladder cancer. Approved PDT photosensitizers are often based on porphyrin or porphyrinoid scaffolds due to their strong absorption in the therapeutic window and high photostability.[50,51] However, recently, a $[Ru(N^N)_3]^{2+}$ complex has completed phase Ib clinical trial as PDT photosensitizer for the treatment of non-muscle-invasive bladder cancer.[52] This prompted the development of PDT photosensitizers beyond organic compounds using metal-based complexes due to the ease of modulation of their photophysical properties. Most reported examples rely on heavy metals such as Ru, Ir, Pt or Re[53] but recent studies demonstrated the potential use of cheaper and more abundant first row metal complexes for phototherapy.[54] To date, most reports of gold-based PDT photosensitizers rely on gold nanoparticles which is beyond the scope of the present review.[55,56] $[Au(TPP)]^+$ (TPP = *meso*-tetraphenylporphyrin) (Figure 4) introduced by Che and colleagues has been demonstrated to have strong cytotoxic activity on various cancer cell lines including nasopharyngal carcinoma and melanoma cells as well as cancer stem cells.[43,57] Its mechanism of action has been investigated in depth and involves the inhibition of mitochondrial chaperone HSP60.[58] Considering the numerous porphyrins and metalloporphyrins for PDT applications, the use of $[Au(TPP)]^+$ and $[Au(TPP)]^+$-based Au(III)/Pt(II) bimetallic complexes (**1**, Figure 4) as PDT agents was explored.[59] Unexpectedly, very low singlet oxygen quantum yields were measured for both gold porphyrins and bimetallic complexes (below 1 %). However, irradiation of $[Au(TPP)]^+$-treated MCF-7 cells at λ_{exc} = 390-420 nm led a 60% reduction of cell viability compared to dark condition. This reduced cell viability was associated with the production of ROS detected by fluorescence microscopy using $DCFH_2$-DA as a probe

demonstrating a small PDT activity of $[Au(TPP)]^+$. Moreover, despite the absence of PDT activity of the Au/Pt bimetallic complex **1**, its cytotoxic activity was improved against MCF-7 breast cancer cell line, as compared to the corresponding Pt-malonato complex.[59] Corroles are a sort of porphyrinoid lacking a *meso* carbon resulting in a smaller chelating site and lower symmetry than porphyrins. Corroles can coordinate various metals in a tetradentate trianionic mode.[60] Interestingly, Au-corrole complexes appeared to have a very different biological behavior compared to porphyrin analogs. Indeed, while the porphyrin-based complex $[Au(TPP)]^+$ presented strong cytotoxic activity in the dark,[43] neutral amphiphilic Au(III) corrole complex **2** (Figure 4) presented a low antiproliferative activity around 100 µM against AY27 rat bladder cancer cells. Moreover, corrole complex **2** could reduce AY27 cells viability by 60 % at a concentration of 10 µM upon 2.5 min of irradiation at 435 nm demonstrating a strong phototoxicity, contrasting with the limited PDT activity of $[Au(TPP)]^+$.[61] Despite these promising results, the investigation of PDT agents based on Au-corroles has not been further developed and they remain mostly used for solar cell construction.[62]

Introduction of an NHC-Au(I) moiety linked to the porphyrin core has been investigated to (1) combine a PDT agent with a chemotherapeutic fragment and (2) enhance the ISC efficiency due the spin-orbit coupling (SOC) of a heavy atom (heavy atom effect). Within this frame, porphyrins *meso*-substituted with NHC-Au-Cl moieties either directly attached to the porphyrin or via a benzyl group have been synthesized (**3a,b**, Figure 4).[63] However, while the corresponding imidazolium salts at 0.5 µM could induce high toxicity when irradiated at 450 and 545 nm for 10 min, neither **3a** nor **3b** did show any phototoxicity on MCF-7 cells. Moreover, while complex **3a** without spacer between the porphyrin and the imidazole rings appeared poorly cytotoxic on MCF-7 cells up to a concentration of 2 µM, at the same concentration **3a** induced 60 % of cell death, highlighting the need of a distance between the photosensitizer and the NHC-Au fragment to induce cytotoxic properties.[63] NHC-Au-Cl fragment has been conjugated *via* a histamine linker to a bacteriopurprinimide (BPI) core (**4**, Figure 4) a photosensitizer absorbing at $\lambda > 800$ nm within the therapeutic window.[64] When tested on PC3 (prostate cancer) and HCT116 (colon cancer) cells, complex **4** demonstrated phototoxicity when irradiated at $\lambda > 720$ nm with IC_{50} values of 101 ± 11 and 96 ± 14 nM respectively, comparable to the BPI-imidazolium precursor and **4** appeared twice more cytotoxic in the dark than its BPI-imidazolium precursor. *In vivo* experiment on PC-3 xenografts demonstrated the quick accumulation of complex **4** in tumors and its excretion after 6 h similarly to its BPI-imidazolium precursor. Moreover, when irradiated at 810 nm, complex **4** induced a higher anti-tumor activity than BPI-imidazolium compound.[64] Fused porphyrin-NHC ligands are a particular class of NHC in which the backbone of the imidazole core corresponds to two adjacent β-positions.[65] Fused porphyrin-NHC-Au-Cl complex **5a** (Figure 4) appeared to be a more efficient photosensitizer for the photo-oxidation reaction of cholesterol than the corresponding tetraarylporphyrin.[66] Similarly, complex **5a** was demonstrated to generate singlet oxygen more efficiently than the corresponding imidazolium salt and tetrarylporphyrin analog. However, similarly to complexes **3a** and **3b**, no particular phototoxicity was observed on MCF-7 cells treated with up to 10 µM of complex **5a**. This lack of activity was attributed to poor complex uptake. Thus, the porphyrin-NHC-Au(I) fragment was conjugated to a mannose moiety through a thiolate linker (complex **5b**, Figure 4). **5b** showed a strong phototoxicity through ROS production with complete cell death at a concentration of 10 µM. Interestingly, the PDT effect of **5b** could be abolished by co-incubation with mannose, suggesting the involvement of mannose receptors in the uptake mechanism of **5b**. Authors also demonstrated the thiolate oxidation to sulfonate by singlet oxygen leading to the release of the thiolate ligand. As such, preservation of complex **5b** from light prior to incubation with cells is of major importance to avoid decomposition of the mannose conjugate, uptake reduction and loss of PDT efficacy.[67] Computational studies have

been carried out on **3a** and **5a** to investigate the impact of the Au(I) cation and its position on the porphyrin ring on SOC of these systems. Calculation showed that, despite the expected heavy atom effect of gold, no particular changes of the SOC constant where observed in both cases due to the absence of involvement of the Au-NHC fragments in the LUMO and LUMO+1 molecular orbitals.[68]

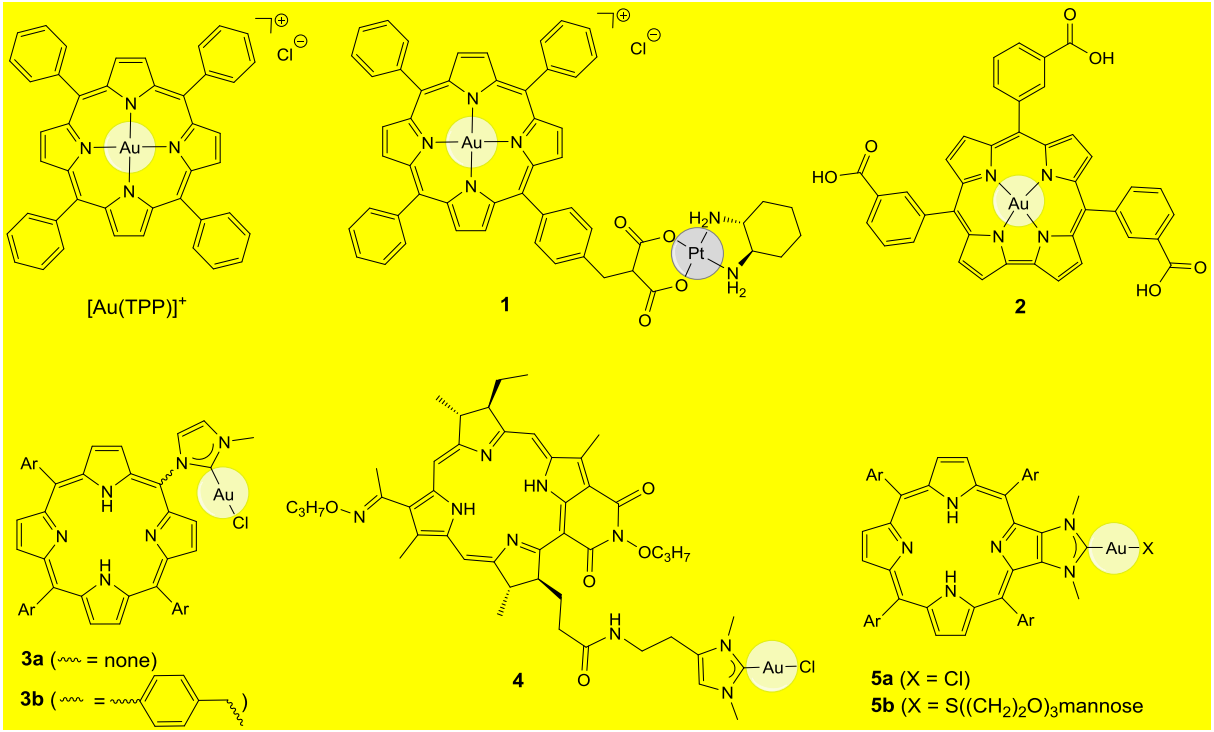

Figure 4. Porphyrinoid-based gold complexes used for PDT

Boron-dipyrromethene (BODIPY) is another well studied class of organic fluorophores with a broad range of applications as fluorescent sensors (pH, metal ion, biomolecules, …)[69] or fluorescent probes for drug uptake studies and intracellular localization.[70] Moreover, BODIPY-based PDT photosensitizers are currently under intense investigation due to their high extinction coefficient, low dark toxicity, resistance to photobleaching and ease of photophysical properties modulation.[71–73] In particular, introduction of heavy atoms such as iodine on the BODIPY core was demonstrated to dramatically enhance the singlet oxygen quantum yield by heavy atom effect.[74] Within this context, an Au(I)-PPh_3 complex conjugated to a BODIPY core through an acetylene linker has been synthesized (complex **6**, Figure 5). This strategy appeared very efficient to promote SOC thanks to the presence of the gold heavy atom as **6** appeared to have very high singlet oxygen quantum yield (Φ_Δ = 84 %, λ_{exc} = 415 nm), even higher than the diiodo-BODIPY photosensitizer (Φ_Δ = 79 %).[75] While in the case of porphyrin-based Au(I) complexes, the Au(I) fragment was not involved in the π-π* transitions responsible for the PDT effect, the alkyne-Au(I) complex extends the π system of the BODIPY core thus participating in the π-π* transitions.[76] Computational studies demonstrated high and very similar inter-system crossing constant for both **6** and the diiodo-BODIPY in agreement with their close and high singlet oxygen quantum yields.[76] **6** was used as PDT agent against A549 lung adenocarcinoma cells and demonstrated strong phototoxicity only when the cells where irradiated at 525 nm at a concentration as low as 2.5 nM, demonstrating the high potential of Au-BODIPY conjugates for PDT applications.[75] Moreover, while [(C^N^C)Au(III)]-alkyne-fluorophore has been demonstrated to have higher inter-system crossing constant than Au(I)-PPh_3 analogs such as **6**,[77] to the best of our knowledge, no Au(III)-alkyne-fluorophore conjugates have been investigated as potential PDT agents.

A limitation of classical photosensitizers is their aggregation-induced quenching at high concentration (achieved upon accumulation in a specific sub-cellular compartment for instance) resulting in a reduced photoactivity. As such, the conjugation of aggregation-induced emission luminogens (AIEgens) for labeling anticancer drugs appears particularly promising. This approach has been recently applied successfully with Au(I)-NHC complexes that preferentially accumulate in cancer cells and induce high TrxR inhibition, resulting in antiproliferative activities in the low micromolar range.[78] Similar approach has been explored for the development of AIEgens-Au(I) PDT agents by coordinating an Au(I)-(C_6F_5) fragment to a triphenylamine benzothiodiazole pyridine (TBP) (complex **7**, Figure 5).[79] **7** was shown to aggregate starting from a fraction of water of 40 % giving rise to a strong emission at 660 nm. In cell culture conditions (99 % water), complex **7** self-assembles in aggregates of 110 nm average size. Interestingly, while TBP ligand is demonstrated to accumulate selectively in lipid droplets,[80] the presence of the Au(I) fragment enhanced the intracellular accumulation in lysosomes.[79] This is in good agreement with previous data showing that the presence of an organic fluorophore could modify the intracellular accumulation site of Au(I)-phosphine complexes,[81] highlighting the need to consider metal-fluorophore conjugates as an independent entity with a behavior differing from their individual constituents. Interestingly, complex **7** appeared mildly cytotoxic *in vitro* in dark condition against HeLa, A549, HepG2 and PC-3 cells but its cytotoxic activity could be improved upon white light irradiation for 30 min. Similarly, complex **7** could trigger ROS production after 8 h incubation in dark condition but this effect was even more pronounced under white light irradiation. This result could be attributed to a combined strong intracellular TrxR inhibition due to the Au(I) fragment associated with efficient photoinduced singlet oxygen generation by the TBP ligand. This synergistic effect between the PDT agent and a chemotoxic Au(I) complex was confirmed *in vivo* on mice bearing subcutaneous xenograft tumors without toxic effects on heart, kidney spleen and liver.[79]

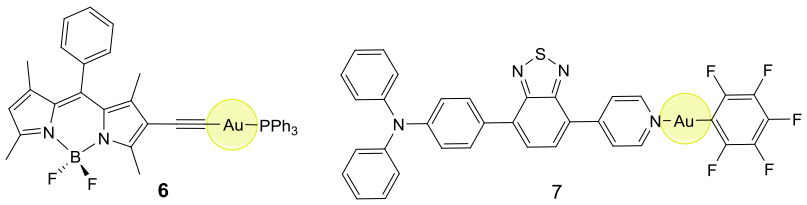

Figure 5. BODIPY- and AIEgen-based gold complexes used for PDT

(C^N^C)Au(III) complexes are reported to have a strong cytotoxic activity against various cancer cells.[8,11,27] This activity can result from the direct coordination of the gold cation onto sulfur-containing proteins and enzymes such as TrxR.[19] This is observed for either neutral complexes with halogens[82] or thiolate ligands[27] or with cationic species with labile ligands such as pyridines[82] or phosphines[83] upon substitution of the coordinated ligand by sulfur atoms of the biological target. On the other hand, cationic complexes with NHC ligands have been shown to be unreactive toward cysteine-containing (poly)peptides such as GSH or TrxR.[41,84] As such, their cytotoxic effect as structural compounds originates from supramolecular interaction such as π-stacking or electrostatic interactions.[36,41] On the contrary, neutral complexes with stable ligands such as alkynyl ligands have been demonstrated to have no cytotoxic effects.[41] [(C^N^C)AuH] complexes, despite being formally metal-hydride complexes, have a very weak hydride reactivity as they were shown to be stable in the presence of acetic acid but could react with strong acids such as trifluoroacetic acid.[85] However, upon outer sphere radical activation, [(C^N^C)AuH] complexes could undergo hydroauration reaction of unsaturated C-C bonds.[86,87] On this basis, Zou and coworkers explored the potential photoactivation of [(C^N^C)AuH] complexes. They demonstrated that while complex **8** (Figure 6) was

perfectly stable in dark conditions, in the presence of pyridinium, acetic acid and N-acetylcysteine (NAC), the corresponding pyridine, acetato and thiolato complexes were obtained upon irradiation at 365 and 420 nm.[88] Computational studies showed that, in dark conditions, energy barriers for the reaction of **8** can be as high as 52 kcal/mol in the case of the reaction with NAC associated with an endergonic formation of the products, preventing this reaction to take place. Upon irradiation, **8** reaches triplet excited state *via* ISC mechanism with distorted geometry. In this triplet state, the gold atom is protruding above the plan of the (C^N^C) pincer causing the elongation of the Au-H bond. From this activated triplet state, the energy barrier is reduced to 15 kcal/mol and the product formation appears exergonic explaining the reaction of **8** under irradiation.[89] Taking advantage of the photoreactivity of complex **8** with thiols, **8** was tested as inhibitor of TrxR. **8** proved to be a potent TrxR inhibitor when irradiated at 365 nm for 5 min with an IC_{50} value of 7.5 ± 1.4 nM on the recombinant enzyme and 1.7 ± 0.6 µM on the enzyme of HepG2 human cancer cells, being comparable to the potent TrxR inhibitor Auranofin.[88] The interaction with cellular proteins was further studied by ICP-MS, revealing an almost four fold higher gold content in HepG2 cells proteins under irradiation compared to dark conditions. Complex **8** appeared cytotoxic when irradiated at 365 nm for 5 min on A549, MCF-7, HepG2 and HCT116 cells with IC_{50} values of 0.9 ± 0.3, 1.3 ± 0.7, 0.6 ± 0.2 and 1.0 ± 0.3 µM, respectively. Moreover, co-incubation of ROS scavengers such as NaN_3 and D-mannitol did not reduce the cytotoxic activity of **8,** suggesting that **8** should act as a PACT rather than a PDT agent. However, a limitation of this system is the high energy wavelength required for activation of the complexes poorly compatible with *in vivo* conditions due to limited tissue penetration. This limitation could be overcome by using two-photon excitation. Indeed, similar phototoxicity was observed under irradiation at 690-700 and at 405 nm.[88]

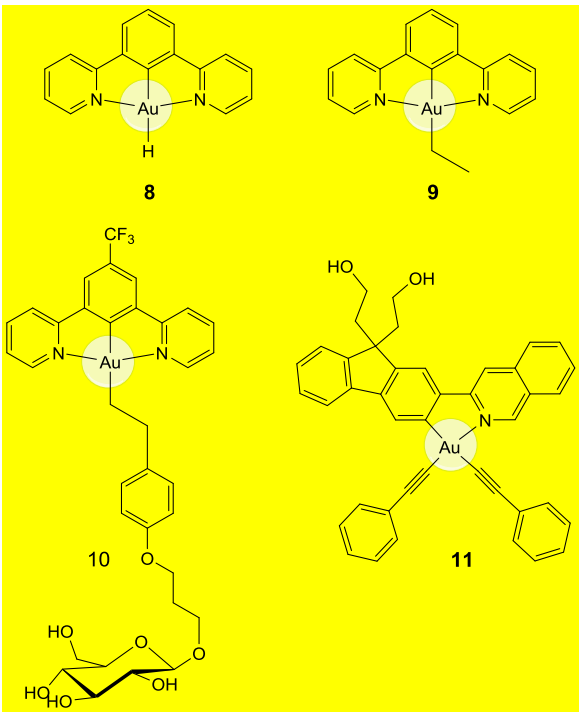

Figure 6. Cyclometalated gold(III) complexes evaluated for PACT and PDT.

β-hydride elimination reactions, although very common in Pd, Pt or Ni chemistry and being an elementary step in many catalytic processes such as in the Heck cross-coupling reaction, remained largely unexplored for Au until the last decade.[90] Zou and coworkers recently demonstrated that [(C^N^C)Au(ethyl/styryl)] complexes such as complex **9** (Figure 6) could undergo β-hydride elimination under irradiation at 365 nm to generate the corresponding hydride complex **8**.[91] Then,

in the presence of an excess of NAC, the photo-generated complex **8** can also be photo-activated (as described before) to generate the corresponding thiolato complex. However, while when starting from complex **8**, the photo-activation stops at the Au-thiolate stage, starting from the alkyl complex **9**, the photo-activation proceeds further with the remaining complex **9** acting as a photosensitizer activating the generated complex **8** undergoing a reductive elimination to form the C-S coupling adduct (CH^N^C-NAC) and an anionic Au(I) complex coordinated by two NAC thiolates which structure is known to have cytotoxic activity.[91] As such, the anticancer property of complex **9** was tested on a panel of human cancer cell lines with IC_{50} under irradiation at 365 nm between 1.4 and 4.6 µM. Similarly to what has been observed for the hydride complex **8**, no particular generation of ROS has been noticed upon irradiation of complex **9** suggesting that the toxic properties might arise from the photo-generation of the dithiolate gold(I) species.[91] Introduction of a glucose moiety *via* a styryl spacer (complex **10**, Figure 6) enhanced the cytotoxic activity of the complex. The amphiphilic complex **10** was shown to self-assemble into round-shape particles of average size 160 nm which uptake mechanism involves endocytosis mediated by glucose transporters. *In vivo*, on mice bearing A375 xenografts, complex **10** significantly reduced the tumor development under 420 nm irradiation without causing particular body weight loss of the treated animals. Similarly to complex **8**, complex **10** could trigger photo-toxicity using two-photon excitation.[91]

Complex **11** (Figure 6) bearing a fluorene-isoquinoline (C^N) cyclometalated ligand and two phenylacetylide ligands has been reported to be completely stable in dark condition for 24 h in the presence of a large excess of NAC while complexes with reduced aromatic (C^N) ligands appeared less stable in the same conditions.[92] Contrarily to what has been observed for (C^N^C)-based complexes **8**-**10**, under irradiation at 420 nm, complex **11** appeared to trigger the formation of singlet oxygen in oxygenated condition. Moreover, in the absence of oxygen and in the presence of thiol, irradiation of complex **11** at 420 nm led to its reduction to a phenylacetylide-Au(I)-thiolate species along with the release of the fluorene-quinoline ligand and the formation of C-S reductive elimination product of NAC with phenylacetylene.[92] This demonstrates that complex **11** could act as both PDT and PACT agent depending on oxygen quantity. These results could be translated to the cellular environment where intracellular $^1O_2$ formation was detected under normoxia and the release of the fluorescent fluorene-quinoline ligand was observed in hypoxic conditions. Complex **11** was tested on various cancer cell lines and showed strong photo-induced activity with IC_{50} values between 0.47 and 1.23 µM under irradiation at 420 nm for 5 min in normoxic conditions. In hypoxic conditions, complex **11** maintained photo-induced activity although reduced by a factor 2 to 5 depending of the considered cell line. Under hypoxia, complex **11** has been shown to very efficiently inhibit TrxR (IC_{50} against cellular enzyme = 3.1 ± 0.6 µM). In normoxia, a 5 min irradiation time appeared necessary to reach efficient inhibition of cellular TrxR (IC_{50} = 3.9 ± 1.1 µM) suggesting that in normoxia both PDT and PACT could take place while in hypoxia only PACT could happen which might explain the differences observed for the cytotoxic activity measured in normoxic and hypoxic conditions. *In vivo* experiments carried out on mice bearing A3475 xenografts treated with 3 $mg.kg^{-1}$ of complex **11** and irradiated at 465 nm showed very promising results with a 92 % tumor growth reduction, no loss of body weight and release of the fluorene-quinoline in tumors suggesting that the photoreduction reaction indeed took place *in vivo*.[92]

3. Gold-mediated selective modification of proteins

While platinum-based drugs are reported to trigger cell death due to intrastrand coordination of the platinum center onto puric bases,[18] gold-based complexes demonstrate their toxic effects mostly *via* enzyme inhibition.[19] In particular, due to their very soft Lewis acid character,

various Au(I) complexes have been reported to efficiently inhibit TrxR, an enzyme responsible for the redox homeostasis of the cells and often overexpressed in cancer cells.[28] By means of mass spectrometry techniques using peptide analogs and biochemical assays,[93,94] it has been demonstrated that the Au(I) complexes inhibited TrxR by selective coordination to the selenocysteine residue located in one of the redox active sites, demonstrating the potential for selective enzyme modification using gold complexes. In the same way, due to their high affinity for sulfur containing ligands Au(III) complexes have been reported to efficiently inhibit cysteine-rich zinc-finger (ZF) enzymes such PARP-1 by replacing the Zn(II) cation from the ZF moiety leading to a conformational change.[31] By means of HPLC-ESI-MS techniques, it could be demonstrated that the benzylpyridine-based (C^N) complex **12** (Figure 7) presented higher affinity for PARP-1 CysCysHisCys ZF than for CysCysHisHis ZFs. After 5 min incubation with the ZFs, adducts with the [(C^N)Au^{III}] fragment were observed.[95]

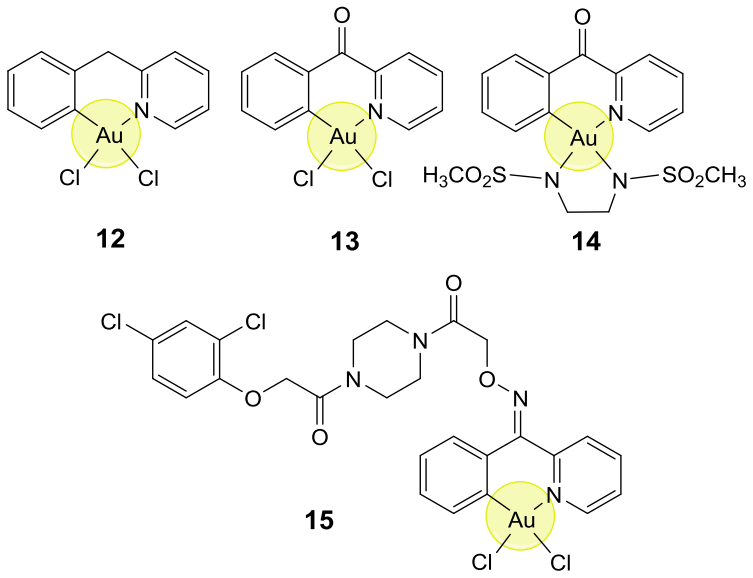

Figure 7. (C^N) cyclometalated Au(III) complexes used for cysteine arylation

Similarly, immediately after mixing, incubation of complex **12** with the HIV nucleocapsid NCp7 presenting two CysCysHisCys ZF domains resulted in the formation of [(C^N)Au^{III}]-F adduct as observed by ESI-MS.[96] However, when the reaction was carried out for 48 h, the appearance of a (C^N)-F adduct was observed which is indicative of the loss of the gold atom and a C-S bond formation by reductive elimination as evidenced by X-Ray absorption spectroscopy (XAS).[96] Although much less described than for Pd(II) and Pt(II) complexes, reductive elimination in Au(III) complexes has been reported in the context for C-C, C-N, C-halogen bond formation.[97] Similar C-S bond formation was observed when **12** was reacted with a CysCysHisHis ZF and with NAC, but, while the fast formation of an adduct between the [(C^N)Au^{III}] fragment and GSH was assessed, no C-S bond formation between the (C^N) chelate and GSH was observed. This demonstrates that the environment of the cysteine plays a role in the reductive elimination reaction.[96] Following these results, a larger panel of [(C^N)AuCl$_2$] complexes including 2-benzoylpyridine, 2-aminophenylpyridine and 2-phenylpyridine was screened as potential arylation agents of a model CysCysHisHis ZF domain after 24 h of incubation in a 3/1 complex/ZF ratio.[98] Variable results were obtained depending of the (C^N) chelate used. While complexes with benzyl- and aminophenylpyridine showed adducts of the ZF with both the [(C^N)Au] fragment and the arylation product, complex **13** with a 2-benzoylpyridine chelate afforded adducts with two and three arylation products. Moreover, in the same conditions, the five-membered (C^N) complex with 2-phenylpyridine ligand did not give any

arylation products. These data highlighted the strong impact of the size of the metallacycle and the nature of the bridge in the (C^N) chelate in the ability of Au(III) complexes to trigger ZF arylation.[98] Such cysteine arylation might be involved in the inhibitory mechanism of PARP-1 by cyclometalated Au(III) complexes.[99] Moreover, while C-S reductive elimination could be demonstrated in the case of (C^N^C)Au complexes,[100] no evidence of its involvement in the anticancer activity of this class of complexes has yet been provided. Theoretical studies were carried out to investigate the differences in C-S bond formation efficiency observed for the different complexes. It has been reported that the first substitution reaction of a chlorido ligand takes place in *trans* position regarding the N-atom of the chelate due to the lower *trans* influence of the N with respect to the C placing the thiolate ligand in *cis* position with respect to the C.[99] However, due to geometrical constraints imposed by the cyclometallation, the C-S reductive elimination is disfavored. At this stage, the N-atom of the pyridine is substituted by a second thiolate ligand leading to the formation of an arylchloridodithiolate anionic complex. In this case, the aryl group can adopt a more favorable conformation enabling the C-S reductive elimination to take place. Calculation revealed that the energetic barriers of both pyridine substitution and reductive elimination steps were the lowest in case of complex **13** rationalizing its higher reactivity observed in the MS experiments.[101] Further studies using cysteine-containing peptides in the middle of the peptide chain and in a terminal position revealed that while in both cases the formation of adducts with the [(C^N)Au] fragments were observed, the arylation reaction did not take place with the terminal cysteine peptide. Calculations showed that, for the arylation to take place, the peptide needs to coordinate in a polydentate way. In a first step, the sulfur of the cysteine along with a nitrogen-containing residue such as asparagine, will chelate the Au(III) center by substituting both chlorido ligands (intermediate **A**, Scheme 1). At this stage, the pyridine ligand has to be replaced by a third residue of the peptide to place the aryl ligand in the favorable conformation for the reduction elimination to occur (intermediate **B**, Scheme 1). As such, the ability of peptides to undergo or not arylation reaction seems to arise from their variable ability to generate and stabilize intermediate **B**.[102]

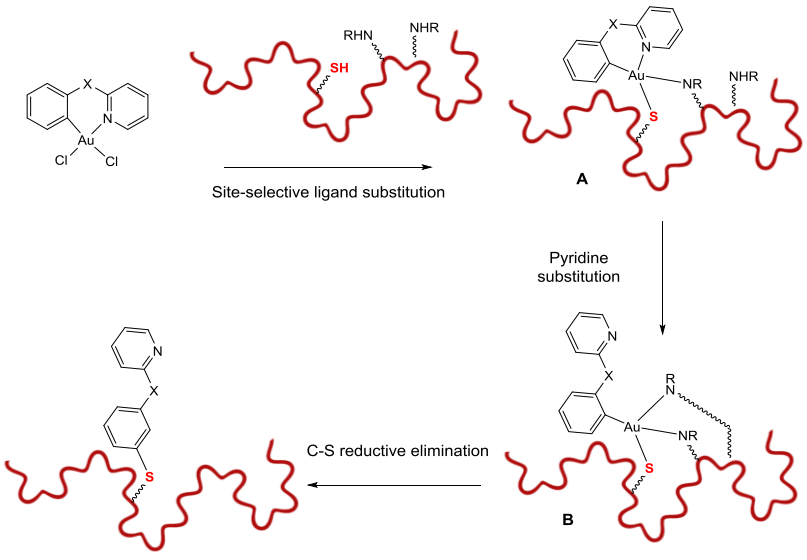

Scheme 1. Proposed mechanism for cysteine arylation reaction with [(C^N)AuCl$_2$] complexes

Taking advantage of its sequence-selective cysteine arylation reaction, complex **13** has been used to perform the global profiling of the arylable cysteines in *Staphylococcus aureus*.[103] *S. aureus* proteome was incubated with 50 µM of complex **13** for 1 h and then with an alkyne-iodoacetamide. A control sample was prepared with only DMSO in the first step and then the alkyne-iodoacetamide.

Both samples were then labeled with desthiobiotin-azide enabling the identification of the cysteines that were modified by **13** by LC-MS/MS technique.[103] As such, 108 cysteines appeared ligandable by **13**, among which were found cysteines from metal- (Zn, Mg and K) and ATP binding sites and from the bacterial thioredoxin reductase, a well-established target of gold complexes.[28] Another identified target was glyceraldehyde-3-phosphate dehydrogenase (GAPDH) a reported target for Ag^+ and Cu^+ cations. Using HR-ESI-MS techniques, the formation of adducts of one of the protein targets with the [(C^N)Au] fragments and arylation products could be demonstrated.[103]

Replacement of the chlorido ligands by an N,N'-bis(methanesulfonyl)ethylenediamine chelate (complex **14**, Figure 7) improved the selectivity for cysteine. This is due to the softer basicity of the sulfonamide ligands with respect to the chlorido ligands disfavoring the substitution by NH_2 residues from lysine or N-terminal of peptides.[104] Using complex **14** as arylating agent, it was possible to perform cysteine-selective functionalization of hexa- to decapeptides with yields up to 99 %. A dansyl ligand was then introduced on the (C^N) chelate by the formation of an oxime function on the bridging carbonyl which was then transferred on the exposed cysteine residues of human and bovine serum albumins, opening the way to site-selective bioconjugation.[104] A similar strategy was used to selectively target the cysteine-containing G12C-mutated KRAS a recognized oncogenic protein. A KRAS-binder was introduced on the (C^N) ligand though an oxime function leading to complex **15** (Figure 7).[105] The KRAS-binder ensure the tight and selective association of **15** with KRAS favoring the interaction of the Au(III) center with the cysteines leading to their arylation. When tested *in vitro* on pancreas and lung cancer cell lines expressing the G12C mutation, complex **15** showed IC_{50} values of 43 ± 1 and 17 ± 4 µM on MiaPaCa and H358 cells respectively while being totally ineffective on H640 lung cancer cells presenting a different mutation of KRAS. Control complex **13** did not show any selectivity demonstrating the importance of the targeting moiety.[105]

Following Bourissou's work about $[(N^P)AuArCl]^+$ complexes (**15,** Figure 7) through the oxidative addition of iodoaryls,[106] Spokoyny used a similar strategy for selective arylation of cysteine derivatives in mild conditions, quantitative yields and short reaction times (Figure 8A).[107] This contrasts with the necessity of reaction time up to 48 h for cysteine arylation by $[(C^N)AuX_2]$ complexes.[96,101,104] When applied to the arylation of GSH, this methodology appeared especially tolerant for the aryl group to transfer as electron-donating and withdrawing groups both led to cysteine arylation with the same quantitative yields. The authors used this methodology to introduce various elaborated moieties such as heterocycles, polymers, fluorescent tags, biotin derivatives and the anticancer drug trametinib.[107] The authors extended the scope of the reaction to mono-cysteine protein functionalization although an increased number of gold complex equivalents was required (20 and 15 equivalents for designed ankyrin repeat protein and fibroblast growth factor 2, respectively).[107] Using di- and tri-cysteine peptides along di- and tri aurated aryl substrates it was possible to form cyclic and bicyclic peptides (Figure 8B). In the same way, by using an excess of GSH, it was possible to decorate by up to 12 peptides poly aurated aryl platforms.[108] Due to the high conversion rate and short reaction time, this methodology was successfully applied for the ^{18}F labelling of various peptides and sugar derivatives including RGD peptides and β-amyloid fragment opening potential application in PET imaging.[109] This demonstrates the great potential of such approach, however therapeutic applications of this methodology have not yet been reported.

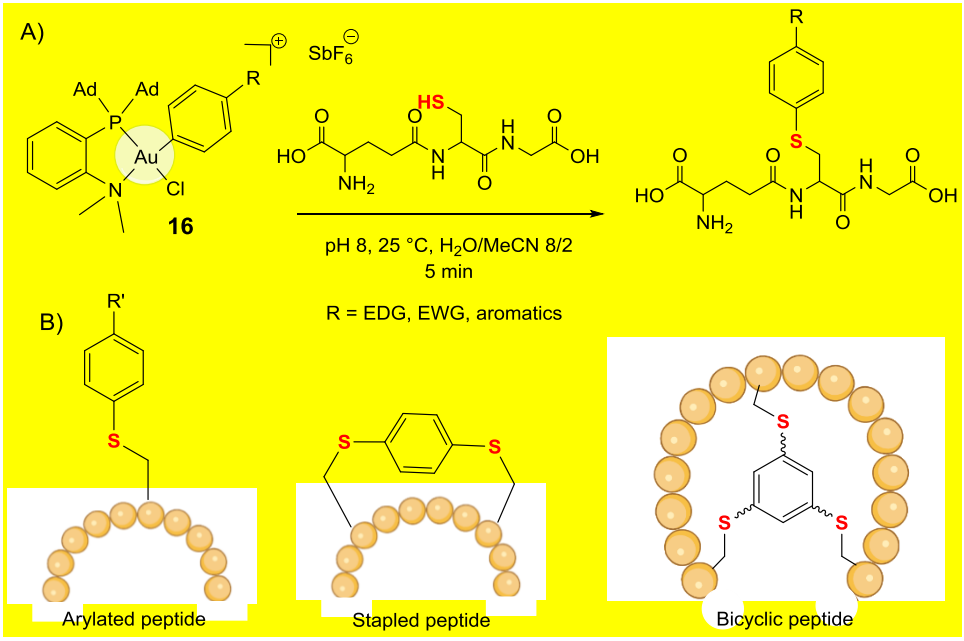

Figure 8. A) GSH arylation conditions using [(N^P)AuArCl]$^+$ complexes B) Peptide structures obtained by this methodology

Gold(III) *meso*-tetraphenylporphyrin [Au(TPP)]$^+$ possesses well-established anticancer properties with IC_{50}s ranging between 33 and 81 nM on a panel of human nasopharyngeal carcinoma cells (SUNE1, HK1, HONE1).[43] Deeper studies on the mechanism of [Au(TPP)]$^+$ revealed strong interactions with various proteins such as the anti-apoptotic protein bcl-2 or the mitochondrial chaperone heat-shock protein 60 (HSP60).[43,58] Although the exact mode of interaction between [Au(TPP)]$^+$ and its targets are not fully disclosed, docking studies point toward non-covalent association relying on electrostatic or π-stacking interactions.[43] Interestingly, the β-substituted gold(III) porphyrin complex **17** (Scheme 2), outperformed the [Au(TPP)]$^+$ complex against various cancer cell lines including ovarian (A2780), lung (NCI-H460), breast (MDA-MB-231) and colon (HCT116) cells along with a reduced toxicity against non cancerous cells.[110] Reactivity studies carried out by mass spectrometry revealed the formation adducts between **17** and various cysteine-containing peptides including GSH and thioredoxin while analogous Zn(II) porphyrin complexes did show only minor formation of the corresponding adducts. This highlights the peculiarity of the Au(III) cation with respect to other transition metals. By means of NMR spectroscopy techniques, the addition of one thiol to the β-position could be demonstrated. Due to this very particular feature, **17** was demonstrated to trigger its anticancer activity *via* the inhibition of various cysteine-containing proteins such as the mitochondrial antioxidant enzyme PRDX3, the protein deubiquitinase UCHL3 and the chaperone HSP90. In all cases, mass spectrometry analysis of reaction between **17** and target-derived peptides revealed the formation of [**17**-peptides] adducts by reaction of the different cysteines. *In vivo* studies on BALB/c mice bearing A2780 and HCT116 xenografts revealed a reduction of the tumor growth by 80 % and 72 % for A2780 and HCT116 xenografts respectively, when treated twice a week for three weeks with **17** (2 mg/kg).[110]

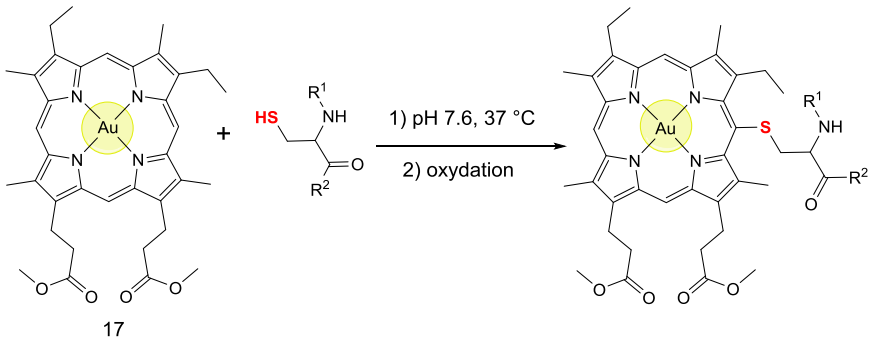

*Scheme 2. Meso addition of cysteine containing proteins on the gold(III)-porphyrin complex **17***

Beyond cysteines, a recent report by Awuah and colleagues described the use of a Au(I) complex to target a lysine of the oncotarget MYC by incorporating a c-MYC affinity ligand onto the [(PR_3)AuCl] structure (**18**, Figure 9A).[111] **18** induced cell death in a c-MYC-dependent manner with up to ten times higher efficacy than the purely organic affinity ligand 10058-F4. Immunoblots studies revealed **18** could induced a higher c-MYC inhibition in treated cells than compound 10058-F4 while the analogous Au(I) complex without the c-MYC affinity ligand substituent had only a limited impact on c-MYC activity. This shows that the presence of the Au(I) complex enhanced the activity of the organic inhibitor. The authors proposed a mechanism for the gold-mediated lysine modification of c-MYC. While bonded to c-MYC the sulfur atom of the thiocarbonyl group of the thioxothiazolidinone can interact with the Au(I) ion making the thiocarbonyl carbon more susceptible to nucleophiles such as amines. Then the Au(I) sulfide can react on the amide carbonyl causing the cleavage of the C-N bond leading to the modification of the lysine by a thiazolone function (Figure 9B).

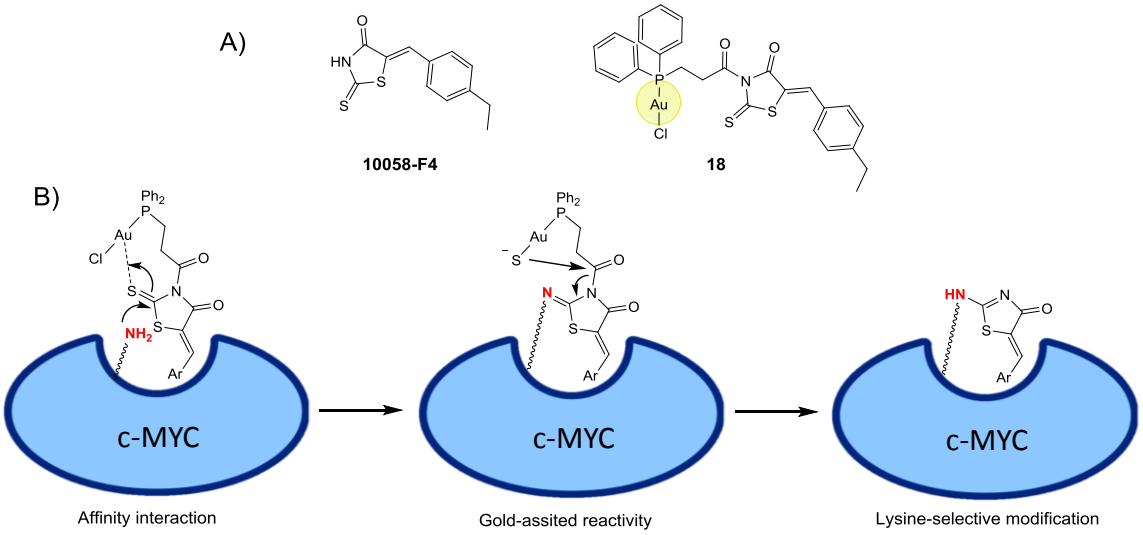

*Figure 9. A) Structures of the c-MYC binder 10058-F4 and its gold-based analog **18**. B) Selective c-MYC inhibition by lysine-selective modification by complex **18**.*

4. Bioorthogonal catalysis with gold-based compounds

The ability to perform / achieve new-to-nature reactions *in vivo* by metal-based catalysis, also simply known as bioorthogonal catalysis, is a truly innovative approach to visualize, manipulate or alter biological processes occurring in cells in a controlled fashion.[112,113] In this field, gold-based compounds currently occupy one of the prominent places, mostly owing to their excellent

biocompatibility. Nevertheless, performing metal-catalyzed reactions in highly complex aqueous media such as cells lysates, cells or even whole organisms is extremely challenging and requires either to properly design and / or formulate the metal species so that its catalytic activity is maintained. This holds particularly true for small molecular gold compounds that can readily be poisoned by sulfur compounds, known to be abundant in biological settings, owing to the formation of strong gold-sulfur bonds.

4.1. Molecular gold catalysts

Cationic gold species display characteristic π-Lewis acidity that translates into the facile coordination to unsaturated bonds, especially alkynes, allowing their functionalization via intra- or intermolecular nucleophilic attack. This unique reactivity leads to a large diversity of functionalized products.[114,115] Besides, gold(I) complexes are tolerant to O_2 and water. Thus, gold species are highly suitable candidates for bioorthogonal catalysis

The first examples of gold-based transformations in cells dealt with chemosensors of Au(III) ions operating by conversion of rhodamine or BODIPY-based profluorescent probes to fluorescent products *via* gold-catalyzed heterocyclization reactions[116–119] or uncaging[120]. One of the most interesting approaches in this area involved the gold(III)-catalyzed hydroarylation (carbocyclisation) of the propargyl ester derivative **A** in protic medium, yielding a blue-fluorescent coumarin derivative (Scheme 3).[121] This strategy inspired Mascareñas and his coworkers who performed a thorough study of the conditions of catalysis. To begin with, they designed the fluorogenic probe **B** to prevent the formation of a mixture of 2 regioisomers occurring upon heterocyclisation of **A**.

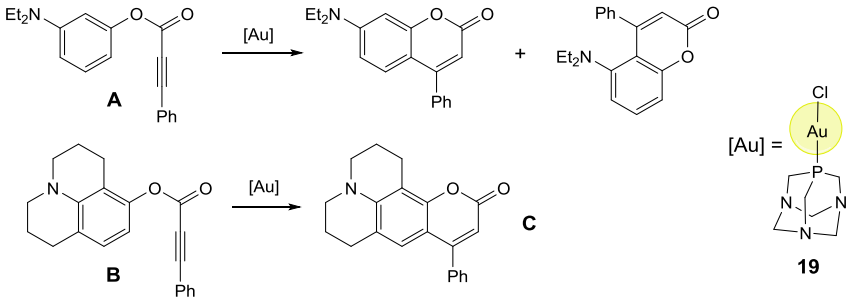

Scheme 3. Gold-catalyzed fluorogenic hydroarylation reactions

They compared the performances of 8 different gold(I) or gold(III) derivatives in the conversion of **B** in aqueous medium and found out that all of them except one gave the coumarin derivative **C** in 65-99% yield. The reaction was transposed to a cellular context (HeLa cells) and the PTA-Au-Cl complex **19** (PTA = 1,3,5-triazaphosphaadamantane), a very well-known ligand in organometallic medicinal chemistry of arene-ruthenium complexes,[122] was found to be the most efficient while inducing the lowest cytotoxicity among the tested compounds. Interestingly, the efficacy of the gold compounds measured from the level of fluorescence was not related to the intracellular concentration of gold measured by ICP-MS.[123]

Tanaka and coworkers exploited the alkynophilic property of gold compounds to catalyze diverse reactions involving terminal alkynes. First, they reported the gold-catalyzed uncaging of pharmacologically active secondary amines via a 6-endocyclisation reaction allowing the removal of the 2-alkynyl benzamide (Ayba) protecting group (Scheme 4). Deprotection of the glycine derivative **Ayba-Gly-OBn** was achieved in very good yield in water-miscible solvents as well as in PBS/DMF 9:1 mixture but required a large amount of $NaAuCl_4$ (50 - 75 mol%). Also, uncaging of the ER antagonist endoxifen from **Ayba-ENDO** was carried achieved in 60 % yield in the presence of 100 mol% NHC

gold complex **20**. Eventually, co-treatment of HeLa, A549 or PC3 cells with caged doxorubicin (**Ayba-DOX**) and 10 µM **coum-Au2** (Figure 10) led to a reduction of the EC_{50} by a factor of 2 to 5 with respect to caged **DOX** alone. However, EC_{50}'s were still 3 to 18 fold higher than those of **DOX** alone.[124]

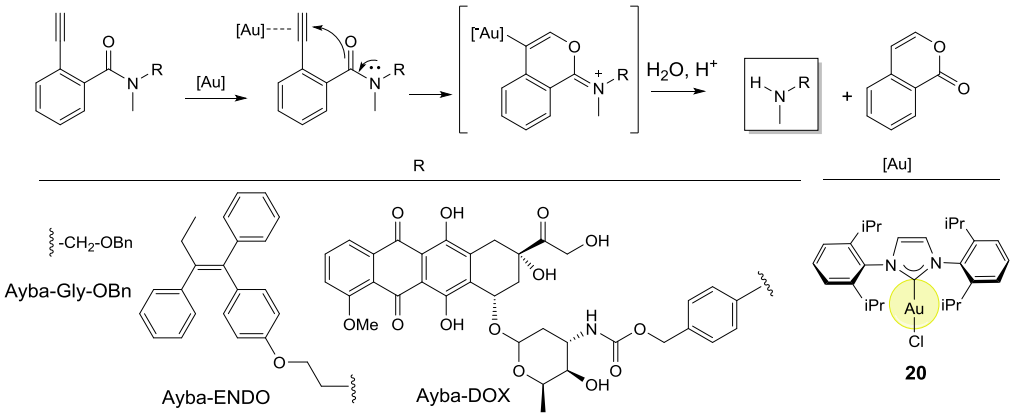

Scheme 4. Uncaging of biologically active secondary amines by gold-catalyzed 2-alkynylbenzamide cyclization

4.2. Artificial metalloenzymes

To protect the gold catalysts from deactivation by cellular thiols, Tanaka and coworkers developed approaches relying on their encapsulation within biopolymers so as to generate artificial metalloenzymes (ArMs). To this aim, they took advantage of the known affinity of coumarin derivatives for albumin[125,126] to generate the ArM **HSA ⊂ coum-Au1** from supramolecular anchoring of **coum-Au1** (Figure 10) to albumin. Effective assembling of **coum-Au1** to the albumin scaffold was evidenced by enhancement of the fluorescence emission of coumarin due to its insertion in the hydrophobic binding pocket located in the subdomain IB of human serum albumin. In a preliminary experiment, fluorescence labeling of the albumin protein host was achieved by addition of **TAMRA-OProp** to the ArM most likely by reaction of lysine residues located in the vicinity of the gold complex.[127]

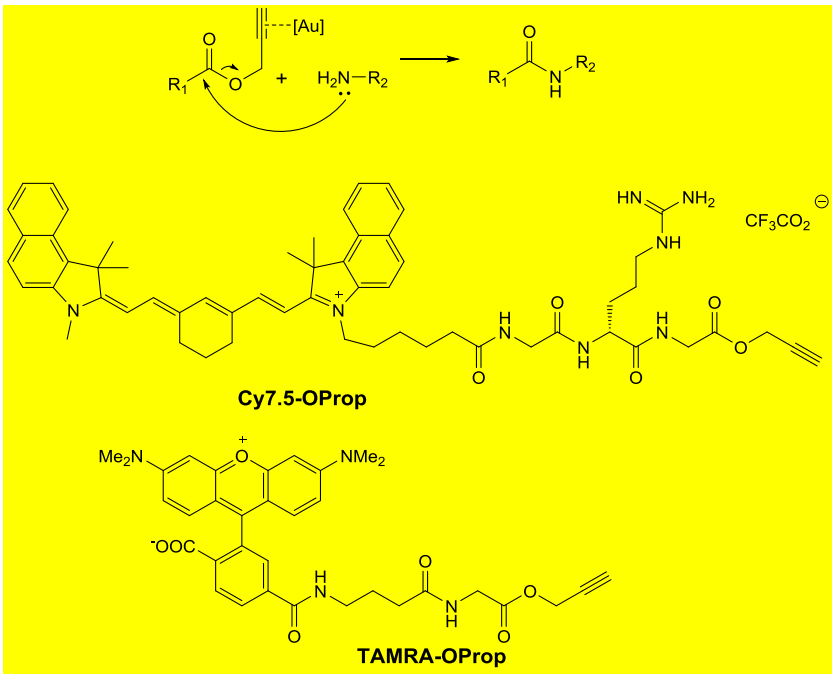

Scheme 5. Mechanism of gold-assisted protein labeling by amide bond formation

This strategy was extended to protein labeling in live mice using N-glycoalbumin scaffolds hosting the gold cofactor **coum-Au1**. These N-glycoalbumins are bioconjugates of human serum albumin and two different glycans whose composition is chosen so as to selectively and rapidly accumulate within the intestine or the liver. These ArMs were independently shown to be poorly cytotoxic on cell cultures and caused no damage to organs *in vivo*.[128] Successive injections of **glycoHSA ⊂ coum-Au1** and the NIR imaging probe **Cy7.5-OProp** to mice resulted in a high level of fluorescence in the corresponding organ as revealed by fluorescence imaging system, while the NIR probe was distributed all over the body upon application of N-glycoalbumin devoid of **coum-Au1**.[129] The mechanism of reaction was assumed to involve gold(III) complex π-coordination allowing the activation of the propargyl ester towards nucleophilic attack by an amine (Scheme 5).

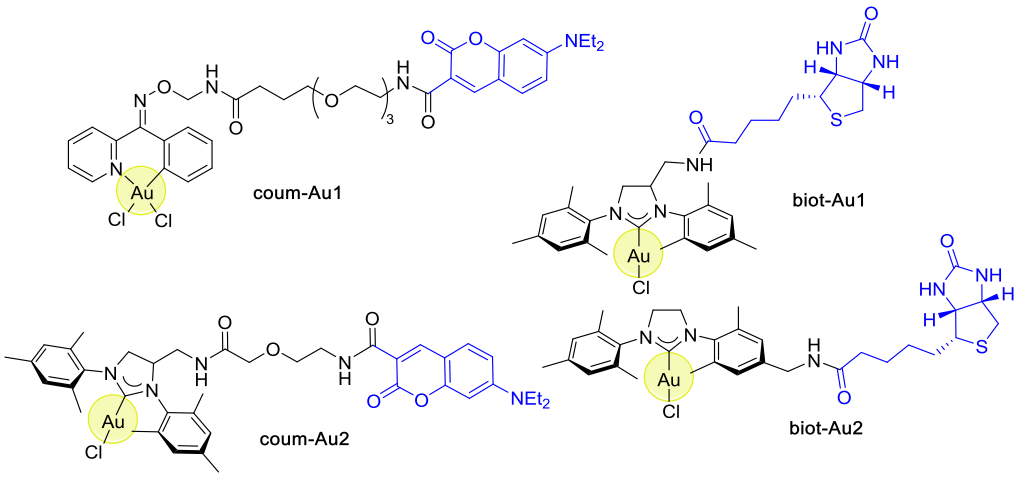

Figure 10. Gold-based cofactors of artificial metalloenzymes

These achievements gave rise to a new concept named Selective Cell Tagging (SeCT) Therapy which is based on the labeling of specific cells with selected chemical moieties (cell surface labeling) *in vivo* to elicit a therapeutic response. The ArM **glycoHSA ⊂ coum-Au1** formed by assembling of N-

glycoalbumin (with α(2,3)sialic acid-terminated glycan) and **coum-Au1** was employed to selectively tag the surface of HeLa cells with the cyclic peptide cRGD to prevent integrin-based cell adhesion to the ECM (extracellular matrix). In a murine model, tumor progression was shown to be considerably slowed down over 4 weeks upon concomitant administration of **glycoHSA ⊂ coum-Au1** and **cRDG-Poc** and the rate of survival was 40% after 81 days whereas, survival rate was 0% under other tested conditions. The same strategy was used to label proteins present at the cell surface with the doxorubicin derivative **DOX-PE** (PE = propargyl ester) (Figure 11), assuming that once **DOX**-labeled proteins are internalized in cells, **DOX** may be released and exert its cytotoxic effect. **DOX-PE** was carefully designed to inhibit its cell uptake. **DOX-PE** also included a cathepsin B cleavage site to facilitate its intracellular release. Derivatization *via* the amino group of **DOX** also ensured a relative innocuity of **DOX-PE**. *In vivo*, successive administration of **glycoHSA ⊂ coum-Au1** and **DOX-PE** to mice led to a significant reduction of tumor growth rate and improvement of animal survival.[130]

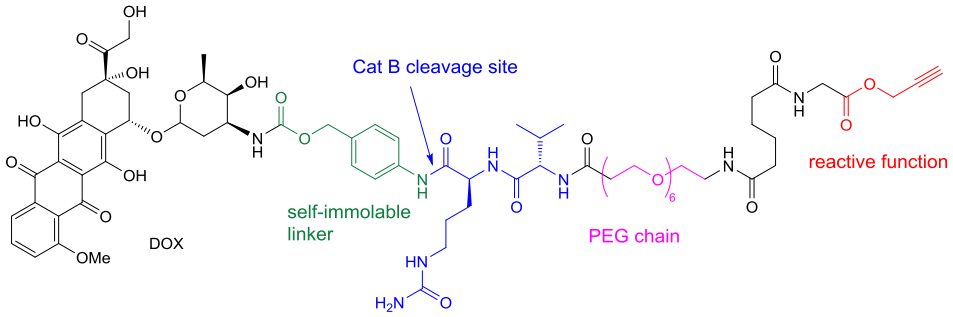

Figure 11. Structure of DOX-PE

The concept of SeCT was also applied to generate an antiproliferative activity by attaching a proapoptotic peptide to proteins at the surface of cancer cells. To this aim, cells in culture were treated with the ArM **cRGD-HSA ⊂ coum-Au1** generated by supramolecular assembling of **coum-Au1** to **cRGD-HSA** conjugate and peptide Ac-GGKLFG-PE. The cRGD motif was meant to target HSA to the cancer cells. This combination induced a marked reduction of SW620 cell viability that was assumed to arise from cell surface protein labeling since neither the **cRGD-HSA ⊂ coum-Au1** nor the peptide were toxic on their own. *In vivo*, the administration of peptide and **cRGD-HSA ⊂ coum-Au1** significantly impaired growth of xenografted tumors in mice and increased their lifetime.[131]

Tanaka and coworkers also reported the design of gold-based ArM for the in-cell synthesis of biologically active molecules structurally similar to natural phenanthridinium alkaloids, known for their DNA intercalating properties.[132] They found out that 5-methyl phenanthridinium **E** could be obtained by gold-catalyzed hydroamination of 2'-ethynyl-N-methyl-2-aminobiphenyl **D** (Scheme 6).

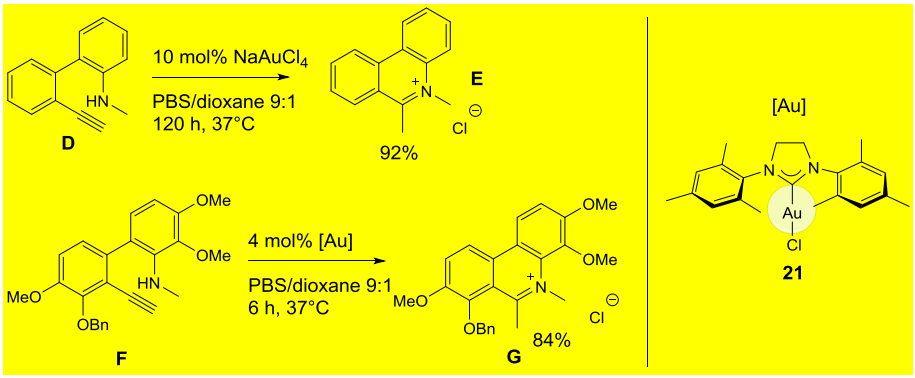

Scheme 6. Synthesis of phenanthridinium compounds by gold-catalyzed heterocyclization reactions

The NHC gold complex **21** outperformed $NaAuCl_4$ since product **E** was obtained in 99% yield after 3 h with only 0.25 mol% catalyst. Intramolecular hydroamination of prodrug **F** was also achieved in 84 % yield in the presence of 4 mol% NHC gold catalyst **21** (Scheme 6). Transposition to the cellular context was then attempted. A549 cells were treated with 8 µM prodrug **F** and 0.6 – 10 µM **coum-Au2**. Concentration-dependent decrease of cell viability was observed to which **coum-Au2** took some part. To alleviate the toxicity arising from the metal catalyst, **coum-Au2** was assembled to HSA by supramolecular anchoring to afford the ArM **HSA ⊂ coum-Au2**. This ArM catalyzed the full conversion of prodrug **D** to **E** in 6 h with 20 mol% catalyst. Besides, the ArM was tolerant to the presence of GSH in the reaction medium while the catalytic activity of the free complex was fully inhibited. Finally, when A549 cells were exposed to 8 µM prodrug **D** and as low as 1.25 µM **HSA ⊂ coum-Au2**, the effect on cell growth was similar to that measured on cells exposed to drug **E** while the prodrug **D** alone had almost no effect.[133]

Tanaka and coworkers also developed a similar strategy to generate dehydropyrrolizidine (DHP) derivatives by gold-catalyzed 5-endo-dig cyclization (hydroamination) of homopropargylamines (Scheme 7).

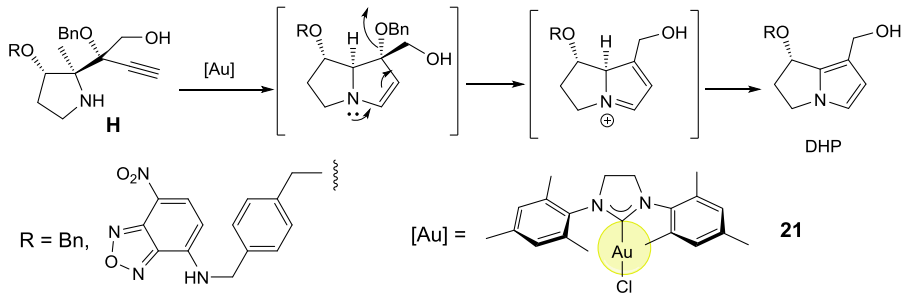

Scheme 7. Synthesis of dehydropyrrolizidine (DHP) by gold-catalyzed heterocyclization reactions

Dehydropyrrolizidines are metabolitically produced from pyrrolizidine alkaloids by CYP450 in the liver and are responsible for their hepatotoxicity and carcinogenicity caused by the high electrophilicity of DHP, giving non specific protein alkylation via Michael addition (Scheme 8).

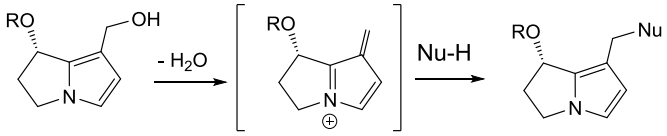

Scheme 8. Mechanism explaining the toxicity of DHP

Indeed, fluorescence labeling of HSA was observed upon its reaction with the NBD cyclisation precursor **H** in the presence of the NHC gold catalyst **21** (Scheme 7). The effect of the mixture of **coum-Au2** and cyclisation precursor **H** on the growth of 3 different cancer cell lines was next studied. It was found that, while precursor **H** was completely inactive (EC_{50}'s of ca. 100 µM), its mixture with **coum-Au-2** led to a significant decrease of the EC_{50}'s although there were not as low as that of DHP itself. The ArM **glycoHSA ⊂ coum-Au2** formed by assembling of **coum-Au2** to N-glycoalbumin (with α(2,3)sialic acid- terminated glycan) was shown to induce a strong cytotoxic effect on SW620 cells in the presence of the cyclisation precursor **H** while their combined effect was moderate on A549 cells and nil on HeLa cells. This selectivity was assumed to be linked to the relative affinities of N-glycoalbumin for the 3 cell lines.[134]

Ward and coworkers also reported the design of gold-based ArMs to catalyze the hydroamination of homopropargylamines. These ArMs are based on the supramolecular association

of streptavidin (Sav) derivatives and 5 different biotin-NHC-Au cofactors. Hydroamination of substrate **I** in the presence of gold catalyst can afford either the quinazoline **J1** from 6-exo-dig cyclisation or/and the indole **J2** from 5-endo-dig cyclisation (Scheme 9). The former one stems from single π-activation by the gold complex while the latter one stems from dual σ,π-activation requiring simultaneous binding of two gold complexes. The tetrameric nature of Sav and the spatial arrangement of the monomers makes theoretically possible the dual activation process leading to the indole product. Accordingly, the ArM formed by wtSav and **biot-Au1** gave exclusively the quinazoline **J1**. Mutation of K121 by A in Sav gave a mixture of quinazolinone **J1** and indole **J2** but the quinazoline **J1** was still the major product (82:18 ratio).

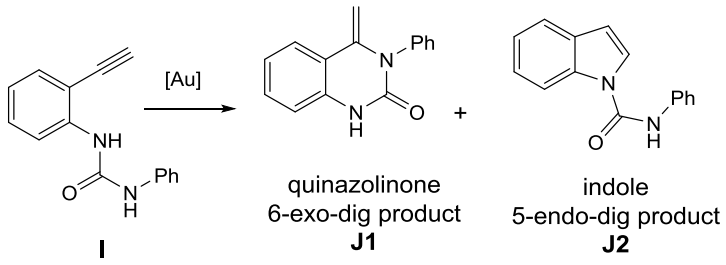

Scheme 9. Gold ArM-catalyzed 6-exo-dig and 5-endo-dig cyclizations of homopropargylamines leading to quinazolinone and indole products

This poor regioselectivity was attributed to the multiple conformations of the biotin cofactor within its binding site. To reduce this flexibility and shield the gold catalyst, a "lid" taken from the dimerization domain of SOD was introduced over the neighboring binding sites of Sav to afford chimeric Sav. With the ArM formed from K121A SOD-Sav and **biot-Au1**, the quinazolinone/indole ratio changed to 62:38. The X-ray structure of SOD-Sav ⊂ **biot-Au1** shows that the gold(I) ions lie 6.5 Å apart from each other (Figure 12), supporting the ability of the ArM to catalyze the hydroamination of substrate **I** by dual σ,π-activation. The SOD-Sav scaffold was then submitted to three successive rounds of directed evolution to eventually identify ArMs giving exclusively quinazolinone **J1** or indole **J2** with high TON.[135]

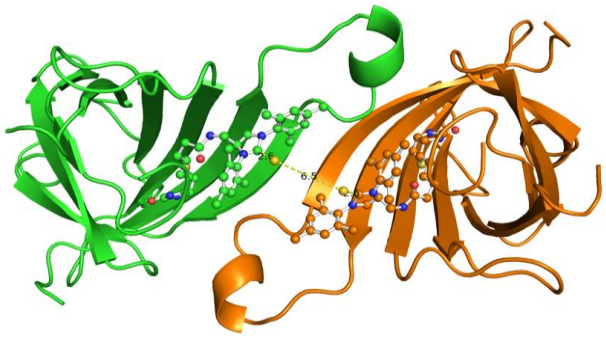

*Figure 12. X-ray structure of K121A SOD-Sav ⊂ **biot-Au1** (two neighboring monomers), Au ions are represented as golden spheres*

By appending the signal peptide of the outer membrane protein A to the sequence of Sav, the same team developed gold-based ArMs operating in the periplasm of *E. coli*. These ArMs were generated by supramolecular anchoring of biotin-NHC-Au cofactors **biot-Au1** and **biot-Au2** (Figure 10) to wtSav or to the library of 400 S112X K121Y Sav mutants. Whole cell screening of the ArM catalytic activity was performed on two model reactions, i.e. hydroamination of 2-ethynylaniline

(Scheme 10) and hydroarylation of the aminocoumarin precursor **A** (Scheme 3). The detrimental effect of thiols on the ArM was bypassed by adding the oxidizing agent diamide. In each case, a double Sav mutant affording 5 to 6-fold increase of TON with respect to the free biotin cofactor was identified by high throughput screening.[136]

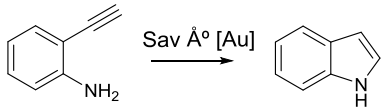

*Scheme 10. Gold ArM-catalyzed hydroamination of 2-ethynylaniline ([Au] = **biot-Au2**)*

4.3. Gold nanoparticles

The catalytic properties of gold nanoparticles (AuNP) have also just lately been implemented for *in vivo* bioorthogonal catalysis. The idea underlying this alternative strategy is eventually to generate a pharmacologically active molecule locally from a prodrug using the nanoparticulate catalyst in the shape of a biocompatible implant. In this condition, side effects due to systemic distribution of the active molecule should be alleviated and its therapeutic index improved. In this field, the Unciti-Broceta team developed several AuNP formulations to uncage biologically active molecules by *O*- or *N*-depropargylation of innocuous precursors.

The first formulation relied on the reduction of $HAuCl_4$ by tetrakis (hydroxymethyl) phosphonium chloride in the presence of 75-µm diameter, amino-functionalized TentaGel™ resin to generate 30 nm-diameter AuNP at the surface of the resin beads. The ability of this first AuNP formulation was first tested on the depropargylation of the rhodamine precursor **Poc-Rh$_{110}$** to release highly fluorescent **Rh$_{110}$** (Scheme 11).

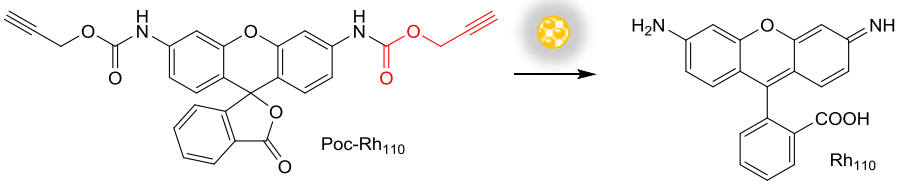

Scheme 11. Gold-catalyzed uncaging of rhodamine 110

Surprisingly, while addition of β-mercaptoethanol completely suppressed the reaction, addition of ethanolamine had the opposite effect. GSH had an ambivalent behavior since it favored the reaction at concentrations up to 50 µM while it progressively quenched the reaction at higher concentration. Next, the AuNP-coated resin was used to uncage 3 different anticancer drugs, namely SAHA, floxuridine and doxorubicin (Scheme 12). In the form of the *O*- or *N*-propargyl derivatives, none of the molecules were cytotoxic. However, in the presence of AuNP-based nanocatalyst, the percentage of A459 cell viability was similar to that reached with the free drugs.

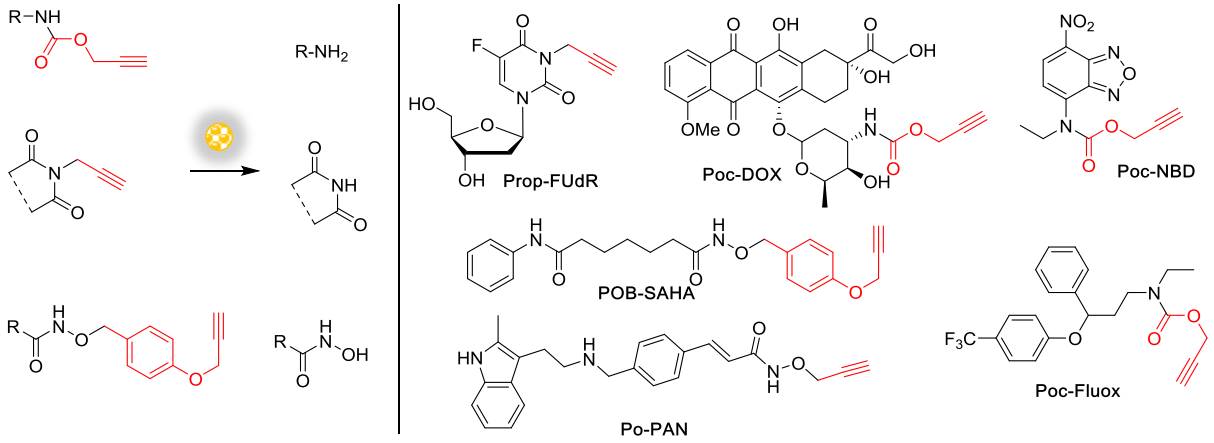

Scheme 12. Gold-catalyzed uncaging of various anticancer drugs

The last part of the study dealt with the implantation of a single AuNP-coated resin bead in the brain of a zebrafish larvae. Exposure of zebrafish to **Poc-Rh$_{110}$** resulted in the generation of fluorescence only in the vicinity of the bead, supporting the relevance of the designed strategy.[137]

In a following piece of work, the same team applied this uncaging strategy to generate the histone deacetylase inhibitor Panobinostat by uncaging of its N-propargyloxy derivative **Po-PAN** (Scheme 12). The preparation of the AuNP-based nanocatalyst was slightly changed to generate smaller AuNP at the surface of the resin beads. The second generation proved to be a little more robust than the first generation and was able to catalyze the release of Panobinostat in cell cultures and induce a significant decrease of A549 cell viability.[138]

A third generation of AuNP-based nanocatalyst was designed where ultrasmall AuNP (ca. 3 nm diameter) were separately synthesized and then loaded under sonication to the positively charged resin beads. This alternative strategy was designed to shield the AuNP and prevent unwanted interactions with proteins or any other biomolecule inactivating its catalytic activity. Indeed, this new formulation enables to perform up to 8 cycles without loss of catalytic activity in the uncaging (depropargylation) of **Poc-NBD** to release green-emitting nitrobenzodioxazole **NBD** (Scheme 12). This new generation of AuNP-based nanocatalyst was then employed to release the antidepressant drug fluoxetine from the carbamate-protected precursor **Poc-Fluox** (Scheme 12) in the central nervous system of zebrafish larvae using an intracranial implant. Exposure of zebrafish to the inactive **Poc-Fluox** resulted in a strong reduction of locomotor activity without inducing any toxicity.[139]

A fourth generation of heterogenous catalyst was formed by encapsulating AuPd nanoalloys in PLGA or mesoporous SiO_2 nanorods (AuPd@PLGA and AuPd@m-SiNR). Both nanocomposites were able to catalyse the depropargylation of **Poc-Rh$_{110}$** (Scheme 11) *in vitro* but AuPd@m-SiNR outperformed AuPd@PLGA. TEM analysis of A549 cells exposed to both types of NP showed a more efficient internalization of AuPd@PLGA with respect to AuPd@m-SiO_2 while "naked" AuPd nanoalloys were not internalized at all. Nevertheless, both nanomaterials were equally able to uncage **Poc-PTX** (Scheme 13) in live A549 cells, leading to the same level of cell viability after 5 days. Generation of **PTX** inside cells was further evidenced by a dramatic change of cell morphology.[140]

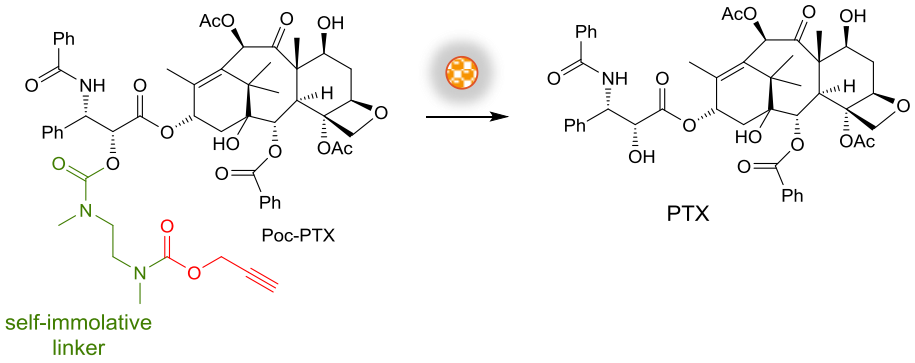

Scheme 13. Gold-catalyzed uncaging of paclitaxel (PTX)

The singular plasmonic properties of AuNP have also been exploited to design biocompatible photocatalytic hybrid nanomaterials able to catalyze reactions *in vivo* upon light irradiation. The first example of the kind was published by Kumar and Lee and dealt with hybrid nanoreactors based on porous silica nanoparticles encapsulating ultrasmall gold nanocrystals (AuNC) and covered with Au nanospheroids. Irradiation of nanomaterial suspension resulted in the rapid increase of temperature due to the well-known hyperthermia process characteristic of plasmonic particles. This hybrid nanomaterial was able to catalyze the uncaging of **Poc-Rh$_{110}$** according to the reaction depicted in Scheme 11 by joint action of AuNC for alkyne activation and Au nanospheroids as light-to-heat converters. These hybrid nanomaterials were efficiently taken up by cells and it was shown that under controlled laser irradiation, rhodamine 110 could be generated *in cellulo* without detrimental effect on cell viability.[141]

Mascareñas and coworkers also devised sophisticated photocatalytic hybrid nanomaterials for bioorthogonal reactions taking place *in cellulo*. These nanostructures involved gold nanorods (AuNR) and TiO_2 NP selected for their respective plasmonic (absorption in the NIR spectral range) and semi-conducting properties, both being encapsulated within mesoporous hollow silica nanospheres (AuNR-TiO_2@hSiNP). The principle underlying the photocatalytic properties of the nanocomposites relies on the NIR irradiation that generates hot electrons which, upon their transfer to the conduction band of the semiconductor, create holes in the Fermi band of the plasmonic particles that in turn confers reduction or oxidation properties to the particles. The cavity of hollow silica nanospheres enables reactions to take place in a confined environment while efficiently protecting the catalyst from deactivation with biological components. As a proof-of-concept, the authors showed that these nanocomposites were able to catalyze the conversion of Rhodamine B to Rhodamine 110 upon NIR light exposure (Scheme 14).[142]

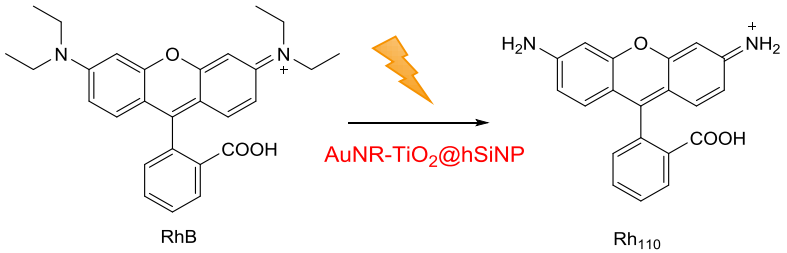

Scheme 14. Light-activated, gold-catalyzed conversion of rhodamine B to rhodamine 110

To sum up, various gold-based species ranging from low molecular weight gold(I) and gold(III) complexes to gold-based artificial metalloenzymes and AuNP-based nanocomposites have been successfully employed to bioorthogonally generate fluorescent or bioactive molecules in the cellular

context and even in whole animals, either by synthesis or release processes. A proper design and formulation of the active species prevented their rapid deactivation by cellular components and ensured their biocompatibility. From the therapeutic point of view, not only innocuous prodrugs are administered but the catalysts design enables drug release only in the side of action. This local delivery is likely to lessen side effects associated to systemic drug delivery.

5. Conclusions and perspectives

This review focused on the emerging therapeutic modalities afforded by gold molecular compounds as well as a few examples dealing with gold-containing nanoparticles. These modalities include the use of gold-based photosensitizers for the generation of ROS, the site-selective protein modification and the gold-based catalysis for the *in cellulo* generation of drugs. These new therapeutic strategies arise from the improved stability of the gold-based structures in physiological medium, enabling the preservation of the structure of the complexes and the development of the analytical methods such as high-resolution mass spectrometry and proteomic methods to uncover their mechanism of action down to the molecular level. These emerging uses of gold-based molecular and nanoparticular systems offer a higher selectivity for cancer cells than classical gold complexes and in some cases by the introduction of biological vectors or enzyme recognition moieties pave the way to the development of gold-based personalized medicines. Moreover, these concepts could be translated in the treatment of other deseases such as microbial, parasitic or viral infections. Although the potential of these approaches has been demonstrated in *in cellulo* up to *in vivo* contexts, the translation of these systems to clinical trials remains the next step to be reached.

Abbreviations

AIE, aggregation induced emission; ArM, artificial metalloenzyme; AuNC, gold nanocrystal; AuNP, gold nanoparticle; AuNR, gold nanorod; DOX, doxorubicin; ER, estrogen receptor; ESI-MS, electrospray ionization mass spectrometry; GSH, glutathione; HSA, human serum albumin; ISC, intersystem crossing; TrxR, thioredoxin reductase; NAC, N-acetyl cysteine; NHC, N-heterocyclic carbene; NIR, near infrared; NBD, nitrobenzodioxazole; PACT, photo-activated chemotherapy; PARP-1, poly-ADP-ribose polymerase 1; PDT, photodynamic therapy; PLGA, Poly(lactic-co-glycolic acid); PTX, paclitaxel; ROS, reactive oxygen species, Sav, streptavidin; SeCT, Selective Cell Tagging; SiNP, silica nanoparticle; SOC, spin-orbit coupling; SOD, superoxide dismutase; TBP, triphenylamine benzothiodiazole pyridine; TPP, tetraphenylporphyrin; ZF, zinc finger

Acknowledgement

Sorbonne Université and the CNRS are kindly acknowledged for financial support.

References

[1] T. G. Benedek, *J. Hist. Med. Allied Sci.* **2004**, *59*, 50–89.
[2] B. M. Sutton, E. McGusty, D. T. Walz, M. J. DiMartino, *J. Med. Chem.* **1972**, *15*, 1095–1098.
[3] R. Oun, Y. E. Moussa, N. J. Wheate, *Dalton Trans.* **2018**, *47*, 6645–6653.
[4] "Study Record | Beta ClinicalTrials.gov," can be found under https://beta.clinicaltrials.gov/study/NCT01419691, **n.d.**
[5] "Study Record | Beta ClinicalTrials.gov," can be found under https://beta.clinicaltrials.gov/study/NCT03456700, **n.d.**
[6] C. Roder, M. J. Thomson, *Drugs R D* **2015**, *15*, 13–20.

[7] C. I. Yeo, K. K. Ooi, E. R. T. Tiekink, *Molecules* **2018**, *23*, 1410.
[8] B. Bertrand, M. R. M. Williams, M. Bochmann, *Chem. Eur. J.* **2018**, *24*, 11840–11851.
[9] A. Tialiou, J. Chin, B. K. Keppler, M. R. Reithofer, *Biomedicines* **2022**, *10*, 1417.
[10] R. T. Mertens, S. Gukathasan, A. S. Arojojoye, C. Olelewe, S. G. Awuah, *Chem. Rev.* **2023**, *123*, 6612–6667.
[11] Y. Lu, X. Ma, X. Chang, Z. Liang, L. Lv, M. Shan, Q. Lu, Z. Wen, R. Gust, W. Liu, *Chem. Soc. Rev.* **2022**, *51*, 5518–5556.
[12] A. Casini, S. R. Thomas, *Chem. Lett.* **2021**, *50*, 1516–1522.
[13] G. Moreno-Alcántar, P. Picchetti, A. Casini, *Angew. Chem. Int. Ed.* **2023**, *62*, e202218000.
[14] C. Ratia, R. G. Soengas, S. M. Soto, *Front. Microbiol.* **2022**, *13*.
[15] M. Navarro, *Coord. Chem. Rev.* **2009**, *253*, 1619–1626.
[16] E. K. Dennis, J. H. Kim, S. Parkin, S. G. Awuah, S. Garneau-Tsodikova, *J. Med. Chem.* **2020**, *63*, 2455–2469.
[17] M. Gil- Moles, U. Basu, R. Büssing, H. Hoffmeister, S. Türck, A. Varchmin, I. Ott, *Chem. Eur. J.* **2020**, *26*, 15140–15144.
[18] D. Wang, S. J. Lippard, *Nat. Rev. Drug Discov.* **2005**, *4*, 307–320.
[19] T. Zou, C. T. Lum, C.-N. Lok, J.-J. Zhang, C.-M. Che, *Chem. Soc. Rev.* **2015**, *44*, 8786–8801.
[20] A. Gutiérrez, I. Marzo, C. Cativiela, A. Laguna, M. C. Gimeno, *Chem. Eur. J.* **2015**, *21*, 11088–11095.
[21] R. Rubbiani, I. Kitanovic, H. Alborzinia, S. Can, A. Kitanovic, L. A. Onambele, M. Stefanopoulou, Y. Geldmacher, W. S. Sheldrick, G. Wolber, A. Prokop, S. Wölfl, I. Ott, *J. Med. Chem.* **2010**, *53*, 8608–8618.
[22] L. Cattaruzza, D. Fregona, M. Mongiat, L. Ronconi, A. Fassina, A. Colombatti, D. Aldinucci, *Int. J. Cancer* **2011**, *128*, 206–215.
[23] A. Casini, M. A. Cinellu, G. Minghetti, C. Gabbiani, M. Coronnello, E. Mini, L. Messori, *J. Med. Chem.* **2006**, *49*, 5524–5531.
[24] R. G. Buckley, A. M. Elsome, S. P. Fricker, G. R. Henderson, B. R. C. Theobald, R. V. Parish, B. P. Howe, L. R. Kelland, *J. Med. Chem.* **1996**, *39*, 5208–5214.
[25] Y. Zhu, B. R. Cameron, R. Mosi, V. Anastassov, J. Cox, L. Qin, Z. Santucci, M. Metz, R. T. Skerlj, S. P. Fricker, *J. Inorg. Biochem.* **2011**, *105*, 754–762.
[26] S. Carboni, A. Zucca, S. Stoccoro, L. Maiore, M. Arca, F. Ortu, C. Artner, B. K. Keppler, S. M. Meier-Menches, A. Casini, M. A. Cinellu, *Inorg. Chem.* **2018**, *57*, 14852–14865.
[27] S. Jürgens, V. Scalcon, N. Estrada-Ortiz, A. Folda, F. Tonolo, C. Jandl, D. L. Browne, M. P. Rigobello, F. E. Kühn, A. Casini, *Bioorg. Med. Chem.* **2017**, *25*, 5452–5460.
[28] A. Bindoli, M. P. Rigobello, G. Scutari, C. Gabbiani, A. Casini, L. Messori, *Coord. Chem. Rev.* **2009**, *253*, 1692–1707.
[29] A. De Luca, C. G. Hartinger, P. J. Dyson, M. Lo Bello, A. Casini, *J. Inorg. Biochem.* **2013**, *119*, 38–42.
[30] V. Milacic, D. Chen, L. Ronconi, K. R. Landis-Piwowar, D. Fregona, Q. P. Dou, *Cancer Res.* **2006**, *66*, 10478–10486.
[31] F. Mendes, M. Groessl, A. A. Nazarov, Y. O. Tsybin, G. Sava, I. Santos, P. J. Dyson, A. Casini, *J. Med. Chem.* **2011**, *54*, 2196–2206.
[32] A. Citta, V. Scalcon, P. Göbel, B. Bertrand, M. Wenzel, A. Folda, M. P. Rigobello, E. Meggers, A. Casini, *RSC Adv.* **2016**, *6*, 79147–79152.
[33] A. de Almeida, A. F. Mósca, D. Wragg, M. Wenzel, P. Kavanagh, G. Barone, S. Leoni, G. Soveral, A. Casini, *Chem. Commun.* **2017**, *53*, 3830–3833.

[34] C. Bazzicalupi, M. Ferraroni, F. Papi, L. Massai, B. Bertrand, L. Messori, P. Gratteri, A. Casini, *Angew. Chem. Int. Ed.* **2016**, 5.
[35] D. Wragg, A. de Almeida, R. Bonsignore, F. E. Kühn, S. Leoni, A. Casini, *Angew. Chem. Int. Ed.* **2018**, *130*, 14732–14736.
[36] J. J. Yan, A. L.-F. Chow, C.-H. Leung, R. W.-Y. Sun, D.-L. Ma, C.-M. Che, *Chem. Commun.* **2010**, *46*, 3893.
[37] R. Rubbiani, S. Can, I. Kitanovic, H. Alborzinia, M. Stefanopoulou, M. Kokoschka, S. Mönchgesang, W. S. Sheldrick, S. Wölfl, I. Ott, *J. Med. Chem.* **2011**, *54*, 8646–8657.
[38] B. Bertrand, L. Stefan, M. Pirrotta, D. Monchaud, E. Bodio, P. Richard, P. Le Gendre, E. Warmerdam, M. H. de Jager, G. M. M. Groothuis, M. Picquet, A. Casini, *Inorg. Chem.* **2014**, *53*, 2296–2303.
[39] F. Guarra, T. Marzo, M. Ferraroni, F. Papi, C. Bazzicalupi, P. Gratteri, G. Pescitelli, L. Messori, T. Biver, C. Gabbiani, *Dalton Trans.* **2018**, *47*, 16132–16138.
[40] S. K. Fung, T. Zou, B. Cao, P.-Y. Lee, Y. M. E. Fung, D. Hu, C.-N. Lok, C.-M. Che, *Angew. Chem. Int. Ed.* **2017**, 6.
[41] B. Bertrand, J. Fernandez-Cestau, J. Angulo, M. M. D. Cominetti, Z. A. E. Waller, M. Searcey, M. A. O'Connell, M. Bochmann, *Inorg. Chem.* **2017**, *56*, 5728–5740.
[42] X.-Q. Zhou, I. Carbo-Bague, M. A. Siegler, J. Hilgendorf, U. Basu, I. Ott, R. Liu, L. Zhang, V. Ramu, A. P. IJzerman, S. Bonnet, *JACS Au* **2021**, *1*, 380–395.
[43] R. W.-Y. Sun, C. K.-L. Li, D.-L. Ma, J. J. Yan, C.-N. Lok, C.-H. Leung, N. Zhu, C.-M. Che, *Chem. Eur. J.* **2010**, *16*, 3097–3113.
[44] S. M. Meier-Menches, A. Casini, *Bioconjugate Chem.* **2020**, *31*, 1279–1288.
[45] W. Niu, X. Chen, W. Tan, A. S. Veige, *Angew. Chem. Int. Ed.* **2016**, *55*, 8889–8893.
[46] J. L.-L. Tsai, A. O.-Y. Chan, C.-M. Che, *Chem. Commun.* **2015**, *51*, 8547–8550.
[47] B. Bertrand, M. A. O'Connell, Z. A. E. Waller, M. Bochmann, *Chem. Eur. J.* **2018**, *24*, 3613–3622.
[48] N. Curado, G. D.-L. Roi, S. Poty, J. S. Lewis, M. Contel, *Chem. Commun.* **2019**, *55*, 1394–1397.
[49] P. Di Mascio, G. R. Martinez, S. Miyamoto, G. E. Ronsein, M. H. G. Medeiros, J. Cadet, *Chem. Rev.* **2019**, *119*, 2043–2086.
[50] J. M. Dąbrowski, B. Pucelik, A. Regiel-Futyra, M. Brindell, O. Mazuryk, A. Kyzioł, G. Stochel, W. Macyk, L. G. Arnaut, *Coord. Chem. Rev.* **2016**, *325*, 67–101.
[51] M. R. Hamblin, *Photochem. Photobiol.* **2020**, *96*, 506–516.
[52] G. S. Kulkarni, L. Lilge, M. Nesbitt, R. J. Dumoulin-White, A. Mandel, M. A. S. Jewett, *Eur. Urol. Open Sci.* **2022**, *41*, 105–111.
[53] X. Zhang, Y. Hou, X. Xiao, X. Chen, M. Hu, X. Geng, Z. Wang, J. Zhao, *Coord. Chem. Rev.* **2020**, *417*, 213371.
[54] L. Gourdon, K. Cariou, G. Gasser, *Chem. Soc. Rev.* **2022**, *51*, 1167–1195.
[55] J. Kadkhoda, A. Tarighatnia, J. Barar, A. Aghanejad, S. Davaran, *Photodiagnosis Photodyn.* **2022**, *37*, 102697.
[56] M. Fan, Y. Han, S. Gao, H. Yan, L. Cao, Z. Li, X.-J. Liang, J. Zhang, *Theranostics* **2020**, *10*, 4944–4957.
[57] C. T. Lum, A. S.-T. Wong, M. C. Lin, C.-M. Che, R. W.-Y. Sun, *Chem. Commun.* **2013**, *49*, 4364–4366.
[58] D. Hu, Y. Liu, Y.-T. Lai, K.-C. Tong, Y.-M. Fung, C.-N. Lok, C.-M. Che, *Chem. Asian J.* **2016**, *55*, 1387–1391.
[59] I. Toubia, C. Nguyen, S. Diring, L. M. A. Ali, L. Larue, R. Aoun, C. Frochot, M. Gary-Bobo, M. Kobeissi, F. Odobel, *Inorg. Chem.* **2019**, *58*, 12395–12406.
[60] S. Nardis, F. Mandoj, M. Stefanelli, R. Paolesse, *Coord. Chem. Rev.* **2019**, *388*, 360–405.

[61] A. B. Alemayehu, N. U. Day, T. Mani, A. B. Rudine, K. E. Thomas, O. A. Gederaas, S. A. Vinogradov, C. C. Wamser, A. Ghosh, *ACS Appl. Mater. Interfaces* **2016**, *8*, 18935–18942.
[62] S.-L. Lai, L. Wang, C. Yang, M.-Y. Chan, X. Guan, C.-C. Kwok, C.-M. Che, *Adv. Funct. Mater.* **2014**, *24*, 4655–4665.
[63] C. Rose, L. Lichon, M. Daurat, S. Clément, M. Gary-Bobo, S. Richeter, *C. R. Chim.* **2021**, *24*, 83–99.
[64] S. Tikhonov, N. Morozova, A. Plutinskaya, E. Plotnikova, A. Pankratov, O. Abramova, E. Diachkova, Y. Vasil'ev, M. Grin, *Int. J. Mol. Sci.* **2022**, *23*, 15776.
[65] S. Richeter, A. Hadj-Aïssa, C. Taffin, A. van der Lee, D. Leclercq, *Chem. Commun.* **2007**, *0*, 2148–2150.
[66] J.-F. Longevial, A. Langlois, A. Buisson, C. H. Devillers, S. Clément, A. van der Lee, P. D. Harvey, S. Richeter, *Organometallics* **2016**, *35*, 663–672.
[67] J.-F. Longevial, K. El Cheikh, D. Aggad, A. Lebrun, A. van der Lee, F. Tielens, S. Clément, A. Morère, M. Garcia, M. Gary-Bobo, S. Richeter, *Chem. Eur. J.* **2017**, *23*, 14017–14026.
[68] S. Scoditti, F. Chiodo, G. Mazzone, S. Richeter, E. Sicilia, *Molecules* **2022**, *27*, 4046.
[69] N. Boens, V. Leen, W. Dehaen, *Chem. Soc. Rev.* **2012**, *41*, 1130–1172.
[70] B. Bertrand, K. Passador, C. Goze, F. Denat, E. Bodio, M. Salmain, *Coord. Chem. Rev.* **2018**, *358*, 108–124.
[71] A. Kamkaew, S. H. Lim, H. B. Lee, L. V. Kiew, L. Y. Chung, K. Burgess, *Chem. Soc. Rev.* **2012**, *42*, 77–88.
[72] J. Zou, Z. Yin, K. Ding, Q. Tang, J. Li, W. Si, J. Shao, Q. Zhang, W. Huang, X. Dong, *ACS Appl. Mater. Interfaces* **2017**, *9*, 32475–32481.
[73] W. Zhang, A. Ahmed, H. Cong, S. Wang, Y. Shen, B. Yu, *Dyes Pigm.* **2021**, *185*, 108937.
[74] T. Yogo, Y. Urano, Y. Ishitsuka, F. Maniwa, T. Nagano, *J. Am. Chem. Soc.* **2005**, *127*, 12162–12163.
[75] M. Üçüncü, E. Karakuş, E. Kurulgan Demirci, M. Sayar, S. Dartar, M. Emrullahoğlu, *Org. Lett.* **2017**, *19*, 2522–2525.
[76] B. C. D. Simone, G. Mazzone, W. Sang-aroon, T. Marino, N. Russo, E. Sicilia, *Phys. Chem. Chem. Phys.* **2019**, *21*, 3446–3452.
[77] K. T. Chan, G. S. M. Tong, W.-P. To, C. Yang, L. Du, D. L. Phillips, C.-M. Che, *Chem. Sci.* **2017**, *8*, 2352–2364.
[78] J. Zhang, H. Zou, J. Lei, B. He, X. He, H. H. Y. Sung, R. T. K. Kwok, J. W. Y. Lam, L. Zheng, B. Z. Tang, *Angew. Chem. Int. Ed.* **2020**, *59*, 7097–7105.
[79] H. Zou, J. Zhang, C. Wu, B. He, Y. Hu, H. H. Y. Sung, R. T. K. Kwok, J. W. Y. Lam, L. Zheng, B. Z. Tang, *ACS Nano* **2021**, *15*, 9176–9185.
[80] X. Shi, S. H. P. Sung, M. M. S. Lee, R. T. K. Kwok, H. H. Y. Sung, H. Liu, J. W. Y. Lam, I. D. Williams, B. Liu, B. Z. Tang, *J. Mater. Chem. B* **2020**, *8*, 1516–1523.
[81] B. Bertrand, P.-E. Doulain, C. Goze, E. Bodio, *Dalton Trans.* **2016**, *45*, 13005–13011.
[82] C. K.-L. Li, R. W.-Y. Sun, S. C.-F. Kui, N. Zhu, C.-M. Che, *Chem. Eur. J.* **2006**, *12*, 5253–5266.
[83] R. W.-Y. Sun, C.-N. Lok, T. T.-H. Fong, C. K.-L. Li, Z. F. Yang, T. Zou, A. F.-M. Siu, C.-M. Che, *Chem. Sci.* **2013**, *4*, 1979.
[84] C. T. Lum, A. S.-T. Wong, M. C. Lin, C.-M. Che, R. W.-Y. Sun, *Chem. Commun.* **2013**, *49*, 4364–4366.
[85] D.-A. Roşca, D. A. Smith, D. L. Hughes, M. Bochmann, *Angew. Chem. Int. Ed.* **2012**, *51*, 10643–10646.

[86] A. Pintus, L. Rocchigiani, J. Fernandez-Cestau, P. H. M. Budzelaar, M. Bochmann, *Angew. Chem. Int. Ed.* **2016**, *55*, 12321–12324.
[87] A. Pintus, M. Bochmann, *RSC Adv.* **2018**, *8*, 2795–2803.
[88] H. Luo, B. Cao, A. S. C. Chan, R. W. Sun, T. Zou, *Angew. Chem. Int. Ed.* **2020**, *59*, 11046–11052.
[89] S. Scoditti, G. Mazzone, E. Sicilia, *Chem. Eur. J.* **2021**, *27*, 15528–15535.
[90] F. Rekhroukh, L. Estevez, S. Mallet-Ladeira, K. Miqueu, A. Amgoune, D. Bourissou, *J. Am. Chem. Soc.* **2016**, *138*, 11920–11929.
[91] J. Jiang, B. Cao, Y. Chen, H. Luo, J. Xue, X. Xiong, T. Zou, *Angew. Chem. Int. Ed.* **2022**, *61*, e202201103.
[92] Y. Luo, B. Cao, M. Zhong, M. Liu, X. Xiong, T. Zou, *Angew Chem Int Ed* **2022**, *61*, e2022126.
[93] A. Pratesi, C. Gabbiani, E. Michelucci, M. Ginanneschi, A. M. Papini, R. Rubbiani, I. Ott, L. Messori, *J. Inorg. Biochem.* **2014**, *136*, 161–169.
[94] B. Bertrand, A. de Almeida, E. P. M. van der Burgt, M. Picquet, A. Citta, A. Folda, M. P. Rigobello, P. Le Gendre, E. Bodio, A. Casini, *Eur. J. Inorg. Chem.* **2014**, *2014*, 4410–4410.
[95] M. N. Wenzel, S. M. Meier-Menches, T. L. Williams, E. Rämisch, G. Barone, A. Casini, *Chem. Commun.* **2018**, *54*, 611–614.
[96] R. E. F. de Paiva, Z. Du, D. H. Nakahata, F. A. Lima, P. P. Corbi, N. P. Farrell, *Angew. Chem. Int. Ed.* **2018**, *57*, 9305–9309.
[97] M. Joost, A. Amgoune, D. Bourissou, *Angew. Chem. Int. Ed.* **2015**, *54*, 15022–15045.
[98] M. Wenzel, R. Bonsignore, S. Thomas, D. Bourissou, G. Barone, A. Casini, *Chem. Eur. J.* **2019**, *25*, 7628–7634.
[99] B. Bertrand, S. Spreckelmeyer, E. Bodio, F. Cocco, M. Picquet, P. Richard, P. Le Gendre, C. Orvig, M. A. Cinellu, A. Casini, *Dalton Trans.* **2015**, *44*, 11911–11918.
[100] L. Currie, L. Rocchigiani, D. L. Hughes, M. Bochmann, *Dalton Trans.* **2018**, *47*, 6333–6343.
[101] M. N. Wenzel, R. Bonsignore, S. R. Thomas, D. Bourissou, G. Barone, A. Casini, *Chem. Eur. J.* **2019**, *25*, 7628–7634.
[102] S. R. Thomas, R. Bonsignore, J. Sánchez Escudero, S. M. Meier- Menches, C. M. Brown, M. O. Wolf, G. Barone, L. Y. P. Luk, A. Casini, *ChemBioChem* **2020**, *21*, 3071–3076.
[103] C. Schmidt, M. Zollo, R. Bonsignore, A. Casini, S. M. Hacker, *Chem. Commun.* **2022**, *58*, 5526–5529.
[104] K. K.-Y. Kung, H.-M. Ko, J.-F. Cui, H.-C. Chong, Y.-C. Leung, M.-K. Wong, *Chem. Commun.* **2014**, *50*, 11899–11902.
[105] S. Gukathasan, S. Parkin, E. P. Black, S. G. Awuah, *Inorg. Chem.* **2021**, *60*, 14582–14593.
[106] A. Zeineddine, L. Estévez, S. Mallet-Ladeira, K. Miqueu, A. Amgoune, D. Bourissou, *Nat Commun* **2017**, *8*, 565.
[107] M. S. Messina, J. M. Stauber, M. A. Waddington, A. L. Rheingold, H. D. Maynard, A. M. Spokoyny, *J. Am. Chem. Soc.* **2018**, *140*, 7065–7069.
[108] J. M. Stauber, A. L. Rheingold, A. M. Spokoyny, *Inorg. Chem.* **2021**, *60*, 5054–5062.
[109] J. W. McDaniel, J. M. Stauber, E. A. Doud, A. M. Spokoyny, J. M. Murphy, *Org. Lett.* **2022**, *24*, 5132–5136.
[110] K.-C. Tong, C.-N. Lok, P.-K. Wan, D. Hu, Y. M. E. Fung, X.-Y. Chang, S. Huang, H. Jiang, C.-M. Che, *Proc. Natl. Acad. Sci. U.S.A.* **2020**, *117*, 1321–1329.
[111] S. Ofori, S. Gukathasan, S. G. Awuah, *Chem. Eur. J.* **2021**, *27*, 4168–4175.

[112] M. O. N. van de L'Isle, M. C. Ortega-Liebana, A. Unciti-Broceta, *Curr. Opin. Chem. Biol.* **2021**, *61*, 32–42.
[113] T.-C. Chang, K. Tanaka, *Bioorg. Med. Chem.* **2021**, *46*, 116353–116353.
[114] H. C. Shen, *Tetrahedron* **2008**, *64*, 3885–3903.
[115] H. C. Shen, *Tetrahedron* **2008**, *64*, 7847–7870.
[116] M. Jung Jou, X. Chen, K. M. K. Swamy, H. Na Kim, H.-J. Kim, S. Lee, J. Yoon, *Chem. Commun.* **2009**, 7218.
[117] H. Seo, M. E. Jun, K. Ranganathan, K.-H. Lee, K.-T. Kim, W. Lim, Y. M. Rhee, K. H. Ahn, *Org. Lett.* **2014**, *16*, 1374–1377.
[118] Y.-K. Yang, S. Lee, J. Tae, *Org. Lett.* **2009**, *11*, 5610–5613.
[119] J.-B. Wang, Q.-Q. Wu, Y.-Z. Min, Y.-Z. Liu, Q.-H. Song, *Chem. Commun.* **2012**, *48*, 744–746.
[120] N. T. Patil, V. S. Shinde, M. S. Thakare, P. Hemant Kumar, Prakriti. R. Bangal, A. K. Barui, C. R. Patra, *Chem. Commun.* **2012**, *48*, 11229.
[121] J. H. Do, H. N. Kim, J. Yoon, J. S. Kim, H.-J. Kim, *Org. Lett.* **2010**, *12*, 932–934.
[122] M. Rausch, P. J. Dyson, P. Nowak-Sliwinska, *Adv. Ther.* **2019**, *2*, 1900042.
[123] C. Vidal, M. Tomás-Gamasa, P. Destito, F. López, J. L. Mascareñas, *Nat Commun* **2018**, *9*, 1913.
[124] K. Vong, T. Yamamoto, T. Chang, K. Tanaka, *Chem. Sci.* **2020**, *11*, 10928–10933.
[125] A. M. L. Zatón, J. M. Ferrer, J. C. R. de Gordoa, M. A. Marquínez, *Chem. Biol. Interac.* **1995**, *97*, 169–174.
[126] A. Garg, D. Mark Manidhar, M. Gokara, C. Malleda, C. Suresh Reddy, R. Subramanyam, *PLoS ONE* **2013**, *8*, e63805.
[127] Y. Lin, K. Vong, K. Matsuoka, K. Tanaka, *Chem. Eur. J.* **2018**, *24*, 10595–10600.
[128] T.-C. Chang, I. Nasibullin, K. Muguruma, Y. Kusakari, T. Shimoda, K. Tanaka, *Bioorg Med Chem* **2022**, *73*, 117005.
[129] K. Tsubokura, K. K. H. Vong, A. R. Pradipta, A. Ogura, S. Urano, T. Tahara, S. Nozaki, H. Onoe, Y. Nakao, R. Sibgatullina, A. Kurbangalieva, Y. Watanabe, K. Tanaka, *Angew. Chem. Int. Ed.* **2017**, *56*, 3579–3584.
[130] K. Vong, T. Tahara, S. Urano, I. Nasibullin, K. Tsubokura, Y. Nakao, A. Kurbangalieva, H. Onoe, Y. Watanabe, K. Tanaka, *Sci. Adv.* **2021**, *7*, eabg4038.
[131] P. Ahmadi, K. Muguruma, T.-C. Chang, S. Tamura, K. Tsubokura, Y. Egawa, T. Suzuki, N. Dohmae, Y. Nakao, K. Tanaka, *Chem. Sci.* **2021**, *12*, 12266–12273.
[132] L.-M. Tumir, M. Radić Stojković, I. Piantanida, *Beilstein J Org Chem* **2014**, *10*, 2930–2954.
[133] T.-C. Chang, K. Vong, T. Yamamoto, K. Tanaka, *Angew. Chem. Int. Ed.* **2021**, *60*, 12446–12454.
[134] M. Kurimoto, T. Chang, Y. Nishiyama, T. Suzuki, N. Dohmae, K. Tanaka, S. Yokoshima, *Angew Chem Int Ed* **2022**, *61*, e202205541.
[135] F. Christoffel, N. Igareta, M. M. Pellizzoni, L. Tiessler-Sala, B. Lozhkin, D. C. Spiess, A. Lledos, J.-D. Marechal, R. L. Peterson, T. R. Ward, *Nat. Catal.* **2021**, *4*, 643–653.
[136] T. Vornholt, F. Christoffel, M. M. Pellizzoni, S. Panke, T. R. Ward, M. Jeschek, *Sci. Adv.* **2021**, *7*, eabe4208.
[137] A. M. Pérez- López, B. Rubio- Ruiz, V. Sebastián, L. Hamilton, C. Adam, T. L. Bray, S. Irusta, P. M. Brennan, G. C. Lloyd- Jones, D. Sieger, J. Santamaría, A. Unciti- Broceta, *Angew. Chem. Int. Ed.* **2017**, *56*, 12548–12552.
[138] B. Rubio-Ruiz, A. M. Pérez-López, V. Sebastián, A. Unciti-Broceta, *Bioorg. Med. Chem.* **2021**, *41*, 116217.
[139] M. C. Ortega-Liebana, N. J. Porter, C. Adam, T. Valero, L. Hamilton, D. Sieger, C. G. Becker, A. Unciti-Broceta, *Angew. Chem.-Int. Edit.* **2022**, *61*, e202111461.

[140] B. Rubio-Ruiz, A. M. Pérez-López, L. Uson, M. C. Ortega-Liebana, T. Valero, M. Arruebo, J. L. Hueso, V. Sebastian, J. Santamaria, A. Unciti-Broceta, *Nano Lett.* **2023**, *23*, 804–811.
[141] A. Kumar, S. Kumar, N. Kumari, S. H. Lee, J. Han, I. J. Michael, Y.-K. Cho, I. S. Lee, *ACS Catal.* **2019**, *9*, 977–990.
[142] A. Sousa-Castillo, J. R. Couceiro, M. Tomás-Gamasa, A. Mariño-López, F. López, W. Baaziz, O. Ersen, M. Comesaña-Hermo, J. L. Mascareñas, M. A. Correa-Duarte, *Nano Lett.* **2020**, *20*, 7068–7076.